THESIS

CONSISTENCY IN THE AMSR-E SNOW PRODUCTS: GROUNDWORK FOR A COUPLED SNOWFALL AND SWE ALGORITHM

Submitted by

Ryan L. Gonzalez

Department of Atmospheric Science

In partial fulfillment of the requirements

For the Degree of Master of Science

Colorado State University

Fort Collins, Colorado

Fall 2019

Master's Committee:

Advisor: Christian Kummerow

Glen Liston
Christine Chiu
Branislav Notaros

ABSTRACT

CONSISTENCY IN THE AMSR-E SNOW PRODUCTS: GROUNDWORK FOR A COUPLED SNOWFALL AND SWE ALGORITHM

Snow is an important wintertime property because it is a source of freshwater, regulates land-atmosphere exchanges, and increases the surface albedo of snow-covered regions. Unfortunately, in-situ observations of both snowfall and snow water equivalent (SWE) are globally sparse and point measurements are not representative of the surrounding area, especially in mountainous regions. The total amount of land covered by snow, which is climatologically important, is fairly straightforward to measure using satellite remote sensing. The total SWE is hydrologically more useful, but significantly more difficult to measure. Accurately measuring snowfall and SWE is an important first step toward a better understanding of the impacts snow has for hydrological and climatological purposes.

Satellite passive microwave retrievals of snow offer potential due to consistent overpasses and the capability to make measurements during the day, night, and cloudy conditions. However, passive microwave snow retrievals are less mature than precipitation retrievals and have been an ongoing area of research. Exacerbating the problem, communities that remotely sense snowfall and SWE from passive microwave sensors have historically operated independently while the accuracy of the products has suffered because of the physical and radiometric dependency between the two. In this study, we assessed the relationship between the Northern Hemisphere snowfall and SWE products from the Advanced Microwave Scanning Radiometer - Earth Observing System (AMSR-E). This assessment provides insight into regimes that can be used as a starting point for future improvements using coupled snowfall and SWE algorithm.

SnowModel, a physically-based snow evolution modeling system driven by the Modern-Era Retrospective analysis for Research and Applications, Version 2 (MERRA-2) reanalysis, was employed to consistently compare snowfall and SWE by accounting for snow evolution. SnowModel has the ability to assimilate observed SWE values to scale the amount of snow that must have fallen to match the observed SWE. Assimilation was performed using AMSR-E, Canadian Meteorological Centre (CMC) Snow Analysis, and Snow Data Assimilation System (SNODAS) SWE to infer the required snowfall for each dataset. Observed AMSR-E snowfall and SWE were then compared to the MERRA-2 snowfall and SnowModel-produced SWE as well as SNODAS and CMC inferred snowfall and observed SWE.

Results from the study showed significantly different snowfall and SWE bias patterns observed by AMSR-E. Specifically, snowfall was underestimated nearly globally and SWE had pronounced regions of over and underestimation. Snowfall and SWE biases were found to differ as a function of surface temperature, snow class, and elevation.

ACKNOWLEDGMENTS

First and foremost, I would like to thank my advisor, Professor Chris Kummerow, for giving me the opportunity to be a part of his research group. We first met in the summer of 2015 during the CMMAP REU program where I conducted undergraduate research at CSU. It was a wonderful experience that drew me back to the Kummerow group and CSU. Many thanks to the current members of the Kummerow group that initially welcomed me and provided assistance along the way to my Master's degree. All the members of the Kummerow group, current and former, are wonderful people and it is a pleasure to be part of that list. A special thank you goes to Glen Liston, Christine Chiu, and Branislav Notaros for agreeing to be a part of my Master's commitee.

To my family who has been curious in what I do during my time at CSU. It's not always easy to explain to them what I do, but their support through thoughtful questions and touching base with me is important. To my girlfriend, Rosemary, who has supported me with my travels across the country for jobs to choosing a Graduate program that is not near home. Her continual love and support has been helped me on a professional and personal level. Thank you.

Lastly, thank you to the CSU Atmospheric Science program that employs brilliant people both personally and scientifically. I have met many friends during my time at CSU that will not be forgotten. The front office staff have been a joy to meet and interact with. They are responsible for many of the things students take for granted, and do so quietly and humbly.

This research has been funded by the award 80NSSC19K0140 titled "Continuity of the AMSR Earth Science Data Records".

TABLE OF CONTENTS

LIST OF FIGURES

CHAPTER 1

Introduction

1.1 Motivation

About one sixth of the world's population depends on snowmelt for their freshwater needs (Barnett et al. 2005). The variability of snow, both interannually and seasonally, impacts water resource management decisions, especially in the agricultural sector. Furthermore, changes in snow-cover significantly alter the land surface albedo that can influence atmospheric processes through energy exchanges in the land-atmopshere system. Progress has been made to better understand these processes, but further information regarding the snow-cover extent and mass is needed. Yet, accurate global estimates of snowfall (snow falling to the ground) and SWE (snow accumulating on the ground) pose a unique set of challenges that currently limit our integrated understanding.

The timing of snowmelt is sensitive to the surface temperatures, whereas the maximum snow accumulation is driven by the snowfall amounts. The latest IPCC report indicates there is higher confidence in the expected trends in surface temperature compared to precipitation in a future climate (Meyer et al. 2014). Changes in surface temperatures have been shown to impact snowpack characteristics such as snow cover onset, snowmelt timing, and snow cover duration (Mote et al. 2005; Liston and Hiemstra 2011). In addition, Zeng et al. (2018) showed both temperature and precipitation control the temporal variability in SWE in the Western United States with correlation coefficients exceeding 0.7 for all regions. They found using temperature alone to predict SWE trends decreases the correlation coefficients to near 0.5 in the Western United States. Masiokas et al. (2006) recognized the impacts of future snowpack change in the Central Andes of Chile and Argentina that provides freshwater to over 10 million people. The authors identified the difficulty in studying snowpack in the Andes due to poor spatial and temporal snowpack observations. Given the uncertainties in future trends of precipitation, an accurate representation of precipitation is even more necessary to assess changes in snowpack characteristics.

Future snowpack changes are expected to pose additional stress to freshwater resources on top of existing water demands from population growth and land-use change. The magnitude of

snowmelt directly impacts livestock production, irrigation for agriculture, fisheries, power generation, municipal use, and recreation. Stewart et al. (2005) estimated the total percentage of runoff generated from snowmelt to be between 50% and 80% in the Western United States. In the same region, current water storage infrastructures are vulnerable to increasing demands on summer water storage because of snowpack changes (Ray 2008; Kaatz et al. 2008). Milly et al. (2005) found future modeled trends of streamflow and water to not be representative of historical observations. Given water management has relied on historical observations of hydrologic variables, future changes in snowpack pose significant challenges to water resource managers and the planning of water storage infrastructure.

In the United States there are two laws that govern water rights. The riparian doctrine covers the East and indicates a person has reasonable rights to use water from a nearby water source such as a lake or stream. The West uses the prior appropriation doctrine that allocates water rights based on the first users of the water. For example, in Colorado many of the more senior water rights are controlled by the agriculture and energy sectors (McNeeley et al. 2016). Colorado state water managers are responsible for regulating the amount of water each party is allowed during period of water shortage. An accurate description of the amount of water stored in snow is an invaluable tool to help decision makers on water storage and usage.

Snowpack has been shown to have important land-atmosphere feedbacks though energy exchanges at the land-atmosphere interface. Many of these exchanges processes have been discussed in Cohen and Rind (1991) and include high albedo, high thermal emissivity, low thermal conductivity, and a sink of latent heat when melting. Studies have shown that snow cover can decrease temperatures throughout the lower troposphere. Walland and Simmonds (1996) found snow cover anomalies have a strong impact on surface temperature and static stability using climate models with a high and low cover scenarios. Using a fully coupled global climate model, Vavrus (2007) found mean annual surface temperatures to be 8-10 K higher in the winter over northern North America and Eurasia when all snow cover was removed. They also found cold-air outbreaks are significantly reduced in frequency because of the inability for cold-air masses to form in high latitude regions. Betts et al. (2014) used in-situ station observation to find the decrease in surface

temperature with snow-cover onset to occur within days of the initial snowfall. They attributed this to the increase in shortwave albedo of snow and the reduction in heat flux from the underlying soil. Snow-cover in the Tibetan Plateau has even been linked to changes in the East Asian Summer Monsoon (Xiao and Duan 2016). They found the local cooling of air due to snow-cover from above normal snow-cover facilitates a strong monsoon season by regulating the moisture transport to the region.

The scale of snow crystals between snowfall and snow on the ground is drastically different. Snow crystals in the atmosphere are highly sensitive to the surrounding air temperature and super-saturation with respect to ice. The snow crystal morphology diagram by Nakaya (1951) shows the main types of snow crystal types, but combinations of these types exist. This diagram made in the 1930's has changed little because of the complexity involved in snow crystal formation. Individual snow crystals range in size between less than 1 millimeter to up to 5 millimeters. Aggregates of multiple snow crystals are typically much larger and can be upwards of 50 millimeters in diameter (NSIDC 2012; Libbrecht 2007). Once snow falls to the surface, the ice crystals undergo constant metamorphism that is sensitive to surface temperature, pressure, humidity, and snowpack temperature gradient. The metamorphism properties influence snow crystal shape, size, snow density, and snow depth. Snow crystals in snowpack have been observed to be highly irregular, but two types of snow crystal shapes that are commonly found in snowpack include rounded snow and faceted snow. Rounded snow occurs when the temperature gradient within the snowpack is weak ($<10^{\circ}$C per 1 m) whereas faceted snow occurs when the temperature gradient is strong ($>10^{\circ}$C per 1 m). Large faceted snow crystals can reach up to 10 millimeters in diameter, but typical snow crystals within a snowpack are on the order of 0.25 to 2 millimeters in diameters. Snow crystals undergo microphysical changes that are sensitive to meteorological variables. Formation and evolution processes of snow crystals are challenging given the sizes of typical crystals.

Snow-cover and snowfall have impacts across a broad range of topics. There is uncertainty in future trends of precipitation, and snow-cover is more sensitive to changes in surface temperature. Water storage infrastructure is vulnerable to earlier onset of snowmelt and water resource managers face pressure of how water should be distributed. Climatologically, snow-cover impacts local

surface temperatures, soil moisture, and precipitation. Snow crystal formation and evolution have been notoriously difficult to accurately identify due to the physical scale of the processes. Accurate observations of snow extent, SWE, and snowfall are increasingly important as the climate changes for hydrological and climatological applications.

1.2 Statement of the Problem

Determining snowfall and snow on the ground at global scales using gauge measurements is challenging. Uncertainty exists in using point measurements to accurately represent the surrounding area because snow can vary significantly on small spatial scales. Many methods have been used to distribute point scale measurements into gridded estimates of snow. Binary regression trees use physical observational variables to predict SWE in complex terrain and have shown varying success (Balk and Elder 2000; Erxleben et al. 2002; Molotch et al. 2005). Binary regression trees require large observational data sets to relate snow properties to physical variables such as elevation, slope, and slope aspect, which inhibits their use for most mountainous observational networks. López-Moreno and Nogués-Bravo (2006) found general additive models (GAMs) to best capture the non-linearity between snow depth and physical predictor variables when distributing point snow depth measurements. GAMs and binary regression trees both perform well in identifying non-linear relationships of snow depth and physical variables, but GAMs have less of a requirement on the number of observational points used. Fassnacht et al. (2003) and Dawson et al. (2016) used linear regression and piecewise linear regression, respectively, to distribute SNOTEL snow depth measurements across different elevation ranges. The piecewise linear regression provides more realistic snow depth distributions by using multiple elevation bins compared to linear regression techniques. These methods have shown success in producing gridded estimates of snow depth that are consistent with observations, but are only applicable to a few regions around the globe, such as the Western United States, with very high gauge density.

Reanalysis products provide a complete description of the water budget for all regions, but there is uncertainty in the representation of snow in reanalyses products (Broxton et al. 2016). Precipitation is the dominant control on land-surface water budgets and most reanalysis rely on the atmospheric general circulation model (AGCM) to generate precipitation. AGCM precipitation

estimates are known to be affected by errors in both the magnitude and timing of precipitation events. Bosilovich et al. (2008) found a majority of widely used reanalyses produce more January precipitation than the Global Precipitation Climatology Project (GPCP) for Northern Hemisphere land cover. Hancock et al. (2014) found three reanalysis forcing datasets underestimate cumulative snowfall by roughly 20 mm compared to the peak SWE amount of the GlobSnow product. While the reanalyses used in these studies are shown to have biases, the uncertainties in the GPCP and GlobSnow products also impact the findings. For example, GPCP and GlobSnow have limitations in orographic regions because of the lack of information provided by in-situ and remote sensing observations. Reanalyses of SWE have been shown to exhibit large spread between datasets due to differences in forcing data, model parameterizations, snow dynamics, and land-surface models (Reichle et al. 2017). Mudryk et al. (2015) found differences in the Noah, Mosaic, Community Land Model (CLM), and Variable Infiltration Capacity (VIC) land surface models to produce varying amounts of SWE. However, they showed the input meteorological forcing data have greater influence on the amount of SWE produced than the differences in land-surface models. A misrepresentation of the initial snowfall can lead to incorrect estimates of snow on the ground and other climate related variables.

Satellite-based passive microwave instruments are playing an increasing role in estimating snow in remote areas because they have the ability to make observations through clouds during daytime and nighttime. Unfortunately, snowfall and snow on the ground have similar microwave scattering signatures that can confuse the corresponding algorithms. Historically, snowfall detection algorithms rely heavily on the use of high frequency channels with a reduced dependency on channels that are sensitive to surface characteristics (Kongoli et al. 2003; Surussavadee and Staelin 2010; Kongoli et al. 2018; You et al. 2017). Yet, recent studies have demonstrated the advantages of combinations of low and high frequency channels to capture surface and snowfall signatures simultaneously. Ebtehaj and Kummerow (2017) and Takbiri et al. (2019) used a k-nearest neighbor approach to separate microwave brightness temperature signatures within different surface classes to better understand brightness temperature patterns for snowfall detection. The probability of snowfall detection for snow covered surfaces was shown to be as high as 0.8 for their method.

Operational passive microwave retrievals of snowfall have been developed using Bayesian and 1-D variational inversion (1DVAR) approaches. The Goddard Profiling Algorithm (GPROF) uses a Bayesian formulation to retrieve surface precipitation and its vertical structure (Kummerow et al. 2015). For precipitation over snow covered surfaces, GPROF uses an *apriori* database of ground-based, radar-observed precipitation together with observed radiometer brightness temperatures. The most-likely solution consists of a weighted sum of database profiles that are radiometrically consistent with the observed brightness temperatures. Another passive microwave snowfall retrieval uses a 1-D variational inversion (1DVAR) based technique (Meng et al. 2017). The retrieval is comprised of the retrieval of cloud properties, ice particle terminal velocity computation, ice water content adjustment, and snowfall rate retrieval. This retrieval has been shown to have a correlation above 0.5 with radar and ground observations in the United States.

SWE algorithms take advantage of the differences in sensitivity to scattering by snow at different frequencies, which was first shown by Ulaby and Stiles (1980). Since then, there have been multiple iterations of passive microwave SWE retrieval algorithms. The spectral difference between the horizontally polarized 18 GHz and 36 GHz channels is commonly related to snow depth. Chang et al. (1987) used a simple linear regression to relate the spectral difference to snow depth. Foster et al. (1997) scaled the Chang et al. (1987) algorithm to account for forest attenuation by dividing the regression coefficient by $(1 - ff)$, where ff is the forest fraction. Kelly (2009) weighted the estimation of forest and non-forest snow by using two spectral differences and varying regression coefficients that are computed using the observed brightness temperatures. The most recent SWE algorithm for the AMSR series, consisting of AMSR-E and AMSR2, uses electromagnetic modeling, climatological snow-cover data, updated density estimates, and artificial neural networks to retrieve SWE from the most-likely set of snow parameters (Tedesco and Jeyaratnam 2016). Despite algorithm updates, SWE remains difficult to retrieve due to limited knowledge of snow microstructure, sub-pixel snow variability, and the inability of microwave radiation to penetrate deep snowpack.

Satellite passive microwave retrievals of snow offer potential to estimate global snow properties due to consistent overpasses and the capability to make measurements during the day, night,

and cloudy conditions, but limitations such as snowfall detection and saturation of signal in deep snowpacks will have to be overcome. Hydrologically, SWE is more important than snowfall, but more severe limitations exist in the retrieval of SWE, especially in deep snowpacks that provide the majority of freshwater from snowmelt. Therefore, because of the physical connection between snowfall and SWE, it is important to identify if and where snowfall measurements can add valuable information to the estimation of SWE. As a first step, this study aims to identify the consistency between the snowfall and SWE products from AMSR-E in order to identify regions that appear in relatively good agreement as well as regions where lack of closure points at significant problems with one or both of the snow products. For the remainder of this paper, snow products refers to both snowfall and SWE. Closure is defined by AMSR-E observing the required amount of snowfall to produce the observed SWE given the snow evolution. The current AMSR-E snow products are not coupled and, unsurprisingly, show significant inconsistencies (Figure 1.1).

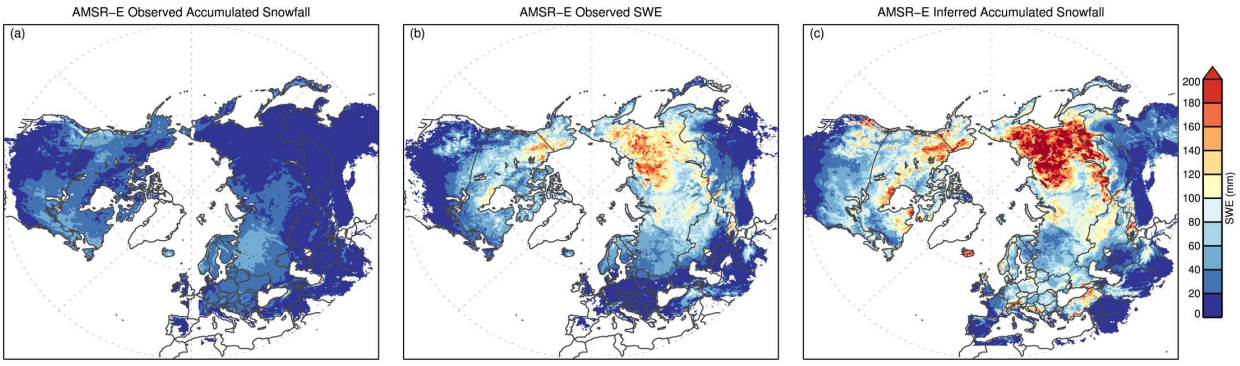

Fig. 1.1. (a) AMSR-E observed accumulated snowfall, (b) AMSR-E observed SWE, and (c) AMSR-E snowfall-based SWE as inferred from SnowModel. Snowfall and SWE amounts are averaged for 8 simulation years 2003-2011. Snowfall is accumulated from the period July-February.

A physically-based snow model, SnowModel, was employed to compare snowfall and SWE in a consistent way by taking into account the snow evolution (Liston and Elder 2006a). Additionally, the Canadian Meteorological Centre (CMC) Snow Analysis and Snow Data Assimilation (SNODAS) snow products were used to provide consistency checks with other widely used SWE

datasets. The methods used to produce each SWE dataset can generate different global distributions of SWE and, as such, it is important to note we do not consider any of the datasets as truth for all regions globally.

The initial snowfall and subsequent SWE can not be compared in a consistent way without accounting for the snow evolution, which is a necessary step within the snow budget. Field campaigns have offered insight into how snowfall and SWE are related to meteorological conditions, but these data are not useful on global scales. Therefore, SnowModel was adapted to the spatial scales of the AMSR-E data in order to identify global uncertainties across the snow lifecycle. The coupling between passive microwave snowfall and SWE using SnowModel is a novel approach used to assess the accuracy and consistency of the snow products. Consistency checks between the snow products provide information about regions of closure and concern and are not interpreted as validation of the snow products. Regions of closure and concern can be used to guide future improvements of the snowfall and SWE algorithms.

CHAPTER 2

Product Description

2.1 AMSR-E Instrument Specifications

This study used observations from the Advanced Microwave Scanning Radiometer - Earth Observing System (AMSR-E). It is a twelve-channel, six-frequency, conically scanning, passive microwave radiometer aboard NASA's Aqua spacecraft. AMSR-E was in a sun-synchronous polar orbit that had equator overpass times of 0130 UTC and 1330 UTC. The instrument began observations in 2002 and stopped rotating in 2011. Geophysical variables related to Earth's water cycle including precipitation rate, cloud water, water vapor, sea surface winds, sea surface temperature, sea ice concentration, snow water equivalent, and soil moisture are all retrieved by AMSR-E. This study focused on the measurement of precipitation rate and snow water equivalent. Table 2.1 provides detailed specifications of AMSR-E.

Table 2.1. Selected sensor specifications for AMSR-E.

Frequency (GHz)	**Polarization**	**Across-Track IFOV (km)**	**Along-Track IFOV (km)**
6.9	V/H	75	43
10.7	V/H	51	29
18.7	V/H	27	16
23.8	V/H	32	18
36.5	V/H	14	8
89.0	V/H	6	4

2.2 Passive Microwave Retrievals of Snowfall

Passive microwave retrievals of precipitation rely on absorption, emission, and scattering interactions with hydrometeor profiles and water vapor. Atmospheric windows below 20 GHz, from 30 to 40 GHz, and at 90 GHz are used to measure rainfall. Frequencies below 20 GHz are sensitive to absorption and emission from hydrometeors and frequencies above 60 GHz are sensitive to scattering from hydrometeors. Higher frequency channels (>90 GHz) provide more information on snow precipitation through ice scattering.

The Goddard Profiling (GPROF) algorithm has a two decade long history of retrieving surface precipitation from passive microwave observations (Kummerow 1994). GPROF is based on a Bayesian method that properly weights an *apriori* database of precipitation profiles and brightness temperatures that are radiometrically consistent with observed brightness temperatures. After the construction of the *apriori* database, a Bayesian inversion methodology is used to solve for the most-likely precipitation rate. The probability of a particular precipitation profile can then be written as:

$$P(\mathbf{R} \mid \mathbf{T_b}) = P(\mathbf{R}) \times P(\mathbf{T_b}|\mathbf{R}) \tag{2.1}$$

where $P(\mathbf{R} \mid \mathbf{T_b})$ is the *posteriori* probability of observing a profile $\mathbf{R}$ given the $\mathbf{T_b}$, P($\mathbf{R}$) is the *apriori* probability a certain profile $\mathbf{R}$ is observed, and P($\mathbf{T_b} \mid \mathbf{R}$) is the probability of making an observation $\mathbf{T_b}$ given the profile $\mathbf{R}$. Computing P($\mathbf{T_b} \mid \mathbf{R}$) requires a radiative transfer model that maps between the profile and brightness temperature space. In the current version of GPROF that is pertinent to snowfall retrievals, the *apriori* database is produced by using coincident radar and radiometer measurements from the Global Precipitation Mission's (GPM) Dual Polarization Radar (DPR) and GPM Microwave Imager (GMI). The formal retrieval solution is solves for the expected value of $\mathbf{R}$ using:

$$\hat{E}(R) = \sum_j R_j \frac{exp[-0.5(Tb_o - Tb_d(R_j))^T (O+D)^{-1} (Tb_o - Tb_d(R_j))]}{\hat{A}} \tag{2.2}$$

where Tb_o is the set of observed brightness temperatures, $Tb_d(R_j)$ are the database modeled brightness temperatures corresponding to the rain rate R_j, O and S are the observational and model error covariance matrices, and $\hat{A}$ is a normalization factor. The formal solution is outlined in Kummerow et al. (1996). Ancillary data helps subset the *apriori* database by 2m temperature, total column water vapor, and land surface classification, which has been shown to positively affect the retrieval. Therefore, the most-likely rain rate is computed by weighting all the database profiles that are within the specified 2m temperature, total column water vapor, and land surface class bin against the observed profile. Currently, surface wet-bulb temperature is used to identify

precipitation phase (Sims and Liu 2015). However, recently there have been studies that used the measured brightness temperatures to determine precipitation phase with good success (Ebtehaj and Kummerow 2017; Takbiri et al. 2019).

The creation of the GPROF *apriori* database for snow-covered land surfaces. Precipitation data from the Multi-Radar Multi-Sensor (MRMS) product was used to build the database by matching radar precipitation pixels with coincident radiometer footprints for snow-covered surfaces. The AMSR-E precipitation rate output is then a weighted precipitation rate of the GMI-MRMS database. Higher weights are computed for more radiometrically consistent observations with the database (i.e. $Tb_o \approx Tb_d(R_j)$).

An alternative approach is used by NOAA to produce a near real-time snow product using passive microwave input from the Advanced Microwave Sounding Unit-A (AMSU-A), Microwave Humidity Sounder (MHS), and the Advanced Technology Microwave Sounder (ATMS). The 1-D variational inversion (1DVAR) based snowfall rate algorithm (SFR) is a physically-based algorithm that consists of snow detection, snowfall rate estimation, and snowfall rate adjustment (Meng et al. 2017). The snow detection algorithm calculates a probability of snow (POS) using a weighted sum of a statistical, satellite-based POS algorithm and a GFS model-based POS algorithm. Each POS algorithm is trained using in-situ observations. The snowfall rate algorithm uses a 1DVAR method to retrieve cloud properties of ice water path and effective size of ice particles. These cloud properties are then used to compute a liquid equivalent snowfall rate assuming the ice particles are exponentially distributed within the cloud. Lastly, the retrieved snowfall rate is adjusted to the National Centers for Environmental Precipitation (NCEP) Stage IV precipitation analysis using quantile mapping.

Retrieving snowfall using passive microwaves is difficult for two main reasons: 1) weak backscattering signal and 2) uncertainties in surface emissivity due to surface snow cover. Microwave frequencies above 60 GHz are more sensitive to ice scattering compared to lower frequencies, and the ice scattering signal highly depends on the microphysical properties of snow crystals (Liu 2008). Microwave modeling of falling snow is difficult because radiative extinction and single-scattering parameters are sensitive to ice particle geometry and the vertical distribution of ice particles in

clouds (Kuo et al. 2016). Ding et al. (2017) created a database of single-scattering properties of 12 ice habits and found there is a significant dependency on temperature for the ice scattering processes in the microwave region. The already weak snowfall microwave signal becomes even weaker as snow accumulates on the ground due to additional scattering from the snowpack. Scattering increases as individual snow grains within the snowpack grow into larger crystals. The evolution of snow grains begin immediately after snow reaches the surface, and growth typically occurs with the age and depth of a snowpack. The increased scattering combined with multiple scattering by the snowpack reduces the surface emissivity compared to a non snow-covered surface. To account for the difference in surface emissivity, GPROF subsets the database by surface class as an attempt to handle precipitation signatures with different surface emissivities. The 1DVAR algorithm does not have the need for *apriori* knowledge of surface emissivity because the inversion algorithm simultaneously solves for the surface emissivity and cloud properties that are consistent in the radiative transfer framework.

2.3 Passive Microwave Remote Sensing of SWE

Snowpack is defined to be the mass of snow on the ground that has been compressed by its own weight. A snowpack can be made of a single layer or multiple layers of snow that are formed by the surrounding meteorological, elevation, and vegetation characteristics. Sturm et al. (1995) defined seasonal snow classifications based on characteristics of the snowpack layers, bulk density, grain size, and crystal morphology. These snow classifications include tundra, taiga, alpine, maritime, prairie, and ephemeral. All types of snowpack consist of a combination of ice crystals and air with the relative volume of ice crystals determining the snow density.

Ulaby and Stiles (1980) identified the capability of using passive microwave sensors for monitoring snow depth and SWE. The ground surface underlying snowpack is known to be a good emitter of microwave radiation, and so a microwave instrument above the snowpack will measure the naturally emitted surface radiation attenuated by the snowpack. Microwave radiation emitted by a dry snowpack is small relative to the radiation emitted from the underlying surface, and therefore is not a large contributor to the total amount of radiation emitted by the snowpack. Dielectric variations between ice and air within the snowpack are responsible for multiple scattering

occurring within the snowpack. Attenuation by the snowpack can then be reduced, in its simplest form, to scattering by individual snow grains that have unique shapes and sizes. The number of snow grains, or scatterers, along the path can then be related to the snow depth. Scattering by the snowpack increases with grain size and frequency (Chang et al. 1987). Increased scattering and multiple scattering within the snowpack allows for an increased chance for microwave radiation to be absorbed leading to an increase in the total amount of attenuation. Given the interactions of microwave radiation within the snowpack, the measured brightness temperature is inversely proportional to the snow depth in dry snow conditions. Liquid water within the snowpack due to rain on snow or snowmelt severely inhibits the ability to estimate snow depth. Liquid water absorbs and emits microwave radiation that will obstruct the scattering signal due to snow grains and, therefore, passive microwaves are only useful to estimate snow depth in a dry snowpack.

Chang et al. (1987) showed microwave frequencies above 25 GHz can detect scattering by the snowpack when SWE amounts exceed roughly 10 mm. Historically, the difference between the 19 GHz and 37 GHz frequencies have been used to determine SWE. For all but the deepest snowpacks, the lower 19 GHz channel is insensitive to the amount of SWE and is used as a baseline brightness temperature against the scattering sensitive 37 GHz channel. Chang et al. (1987) used a simple linear regression with a regression coefficient of 1.6 cm K^{-1} to relate the spectral difference to snow depth. A constant density of 0.3 g cm^{-3} was then used to derive SWE. In the microwave region, vegetation is a strong absorber at 37 GHz so Foster et al. (1997) scaled the Chang et al. (1987) algorithm to account for forest attenuation by dividing the regression coefficient by $(1 - ff)$, where ff is the forest fraction. Including surface vegetation information was shown to improve SWE estimate compared to a snow depth climatology than previous algorithms.

The current, operational AMSR-E SWE algorithm uses a similar linear regression method, but includes more complexity surrounding issues regarding vegetation, snow grain size, and deep snowpacks (Kelly 2009). Four ancillary datasets are incorporated into the AMSR-E SWE algorithm and include data of snow probability, forest fraction, forest density, and snow density. The AMSR-E SWE algorithm is comprised of four parts: snow detection, snow depth estimation, snow depth retrieval and snow depth conversion to SWE. Snow detection and snow depth estimation are

performed using numerous brightness temperature threshold tests. A flow chart of the full AMSR-E SWE algorithm including the brightness temperature thresholds can be found in Tedesco and Jeyaratnam (2016). If moderate to deep snow is detected, then snow depth retrieval is performed separately for forest covered area and non-forest covered area using Equation 2.3:

$$SD = ff \times (SD_{ff}) + (1 - ff) \times (SD_{nff}) \tag{2.3}$$

where SD is snow depth, SD_{ff} is snow depth for forest covered area, and SD_{ff} is snow depth for non-forest covered area. SD_{ff} and SD_{ff} are calculated using Equation 2.4 and 2.5:

$$SD_{ff} = \frac{1}{log_{10}(Tb_{36V} - Tb_{36H})} \times \frac{Tb_{18V} - Tb_{36V}}{1 - 0.6fd} \tag{2.4}$$

$$SD_{nff} = [\frac{1}{log_{10}(Tb_{36V} - Tb_{36H})} \times (Tb_{18V} - Tb_{36V})] + [\frac{1}{log_{10}(Tb_{18V} - Tb_{18H})} \times (Tb_{10V} - Tb_{18V})] \tag{2.5}$$

where fd is the forest density. The retrieval coefficients ultimately account for the spatiotemporal variability of changing snow grain sizes in the observed snowpack. The retrieval coefficients are dynamic and decrease with increasing snow depth to account for the growth of snow grains throughout the snow accumulation season. They are a first attempt to account for changing snowpack characteristics and try to inhibit the overestimation of snow depth for snowpacks with larger snow grains (Kelly 2009). However, Tedesco and Narvekar (2010) showed the retrieval coefficients are uncorrelated with the microwave effective grain size obtained from an electromagnetic snow model. Finally, snow depth is converted to SWE using a spatially varying snow density data set based on the snow surface climate classes outlined in Sturm et al. (1995).

2.4 SnowModel

SnowModel, a spatially distributed snow-evolution model, includes the first-order physics required to simulate snow processes in landscapes and climates where snow occurs (Liston and Elder 2006a). For this study, SnowModel was used to link the initial snowfall and subsequent SWE from

AMSR-E, CMC, and SNODAS through estimates of snow evolution. It is designed to run on high spatial-temporal resolutions, but can be run on coarser spatial resolutions if the loss of high resolution information is tolerable. Processes simulated include snow accumulation; snow density evolution; snowpack compaction, sublimation, and melt; forest canopy snow interception, unloading, and sublimation; and wind-driven snow redistribution and sublimation. Required inputs are temporally-varying fields of meteorological forcing data and spatially-varying fields of topography and vegetation.

SnowModel is a collection of five coupled submodels that each simulate different physical processes known to drive snow evolution: MicroMet, EnBal, SnowPack, SnowTran-3D, and SnowAssim. At each timestep, meteorological forcing data are distributed over the entire domain using MicroMet and then at each gridcell the following processed are simulated: 1) perform near-surface energy balance calculations using EnBal, 2) evolve the snowpack defined by the melt and precipitation input using SnowPack, and 3) transport snow by wind-driven processes using SnowTran-3D.

Following the completion of the entire simulation, the snow assimilation submodel, SnowAssim, can be used to constrain the modeled SWE output to match the observed SWE. SnowAssim uses the assimilated SWE data to scale the modeled precipitation and melt. Running the SnowAssim submodel requires two SnowModel runs: an initial run to evolve snow according to the meteorological forcing data and a second run with the scaled precipitation and melt. SnowAssim provides an updated precipitation amount that will produce the observed SWE during the second SnowModel simulation.

SnowModel has been found to be useful across a broad range of environments, but there are limitations that exist within the model that effect the output (G. Liston 2018, personal communication). A large uncertainty in the model includes the assumption of homogeneous grid cell processes and vegetation as subgrid-scale processes are not accounted for. This assumption is more valid when running the model on smaller spatial scales. For example, snow distribution processes in forested regions as well as wind-driven snow processes occur at spatial scales of one to hundreds of meters. The precipitation and temperature distributions across large elevation ranges are strongly linked to the assumed temperature lapse rates and precipitation scaling factors. These

relationships are important to defining snow accumulation and melt across elevation ranges. The cloud cover is defined by converting the surface air temperature and relative humidity to values at 700mb and then computing the cloud fraction. This definition does not always apply to the given meteorological variables such as under strong radiational cooling under clear skies that increase the surface relative humidity.

2.4.1 MicroMet

MicroMet is a quasi-physically based, high-resolution meteorological distribution model (Liston and Elder 2006b). MicroMet is designed to produce high-resolution meteorological forcing data needed to run terrestrial models. It is a data assimilation scheme that can interpolate station observations, remote sensing data, and gridded reanalysis or model data from an irregular or regular grid. Known physical relationships between forcing data and topography are used to better distribute the forcing data across the surrounding landscape. MicroMet has been used extensively to create high-resolution data across a variety of climate regimes including Colorado, Wyoming, Idaho, Alaska, Greenland, and Antarctica. A preprocessor is included to correct deficiencies in the data or fill missing data in order to provide continuous forcing data to the model. Interpolation is performed using a Barnes objective analysis scheme with a Gaussian distance-dependent weighting function. Modern-Era Retrospective Analysis for Research and Applications, version 2 (MERRA-2) reanalysis is used to force SnowModel. MERRA-2 is interpolated onto the SnowModel grid using a nearest-neighbor approach so the Barnes interpolation scheme within MicroMet is not used. MERRA-2 is the latest atmospheric reanalysis within NASA's Global Modeling and Assimilation Office (GMAO) and is an improvement on the original MERRA reanalysis. MERRA's original goal was to improve the representation of the global water cycle while accounting for the plethora of NASA Earth Observing System (EOS) platforms. MERRA-2 contains improvements to the Goddard Earth Observing System (GEOS) model as well as the assimilation system. The value of using MERRA-2 to force SnowModel is continuous meteorological forcing data that assimilates satellite measurements as well as more conventional radiosonde and surface observations.

2.4.2 EnBal

EnBal computes surface energy balances in response to near-surface meteorological variables provided by MicroMet (Liston 1995). Equation 2.6 is used to calculate surface latent and sensible heat fluxes as well as available energy for snow melt.

$$(1-\alpha)Q_{si} + Q_{li} + Q_{le} + Q_h + Q_e + Qc = Qm \tag{2.6}$$

where *si* is the solar radiation reaching the surface, *li* is the longwave radiation reaching the surface, *le* is the emitted longwave radiation, *h* is the sensible heat exchange, *e* is the latent heat exchange, *c* is the conductive energy transport, *m* is the energy available for melt, and α is the surface albedo. The value of this equation is that each component can be solved for using relationships with surface temperature only. The energy for melting is initially set to zero and the surface temperature is solved for iteratively. However, when snow is present and the surface temperature is above zero celsius, there is excess energy that can be used for melting. This melt energy is solved for by setting the surface temperature to zero celsius to compute the melt energy.

2.4.3 SnowPack

SnowPack is a single layer, snowpack evolution model (Liston and Hall 1995). It defines changes in the density and depth of the snowpack given the precipitation and melt characteristics provided by MicroMet. SnowPack physically evolves snow density in two ways. The first evolves snow density throughout the season in response to the snowpack temperature gradient and compaction from the weight of the overlying snowpack. The second method redistributes snow meltwater throughout the snowpack until a maximum density is achieved, and the remaining free water is considered to be runoff. Density evolution from additional accumulation and compaction follows calculations from Anderson (1976). Snow depth change from sublimation computed in EnBal is also accounted for in SnowPack.

2.4.4 SnowTran-3D

SnowTran-3D is a three-dimensional model that simulates snow evolution from wind driven snow processes (Liston and Sturm 1998). SnowTran-3D has the ability to simulate numerous wind-driven snow processes including the transport and sublimation of suspended and saltated

snow. Each SnowModel gridpoint has a vegetation type with a specific snow holding depth that must be exceeded in order for snow to be available for transportation by the wind. The basic component of the model is a spatio-temporal mass balance equation driven by the deposition and erosion of snow. SnowTran-3D is not employed in this study, and snow transport processes are not simulated. Given the regional nature of this study, this is not expected to impact the results.

2.4.5 SnowAssim

SnowAssim uses in-situ or remotely sensed SWE data to constrain the modeled outputs of snowfall (Liston and Hiemstra 2008). Deficiencies in SnowModel can be contributed to limitations in the snow physics, uncertainties in meteorological data, topography, and vegetation. Model simulated errors are defined to be the difference between observed SWE and modeled SWE. The errors are used to create corrections that are then applied in a second SnowModel run and retroactively create SWE distributions that match the assimilated SWE. SnowAssim is computationally inexpensive and provides SWE improvements throughout the entire snow season. Because precipitation is the dominant control on snow accumulation, SnowAssim adjusts snowfall using SWE observations. Uncertainty in snowfall is the largest source of error in modeling snow on the ground (Raleigh et al. 2015). This justifies the assimilation of SWE observations rather than snowfall observations. Furthermore, the assimilation of SWE can provide updated estimates of snowmelt during the ablation portion of the winter season.

The submodel is able to determine if accumulation or ablation should be scaled by calculating the relative contribution of snowfall or melt during the assimilation period. The model determines which process is dominant for the assimilation period by computing the relative contribution of the accumulation and melt during the observation interval using,

$$ {}_{t-1}^{t}\mathrm{R}_{\mathrm{precip}} = \frac{\sum_{t-1}^{t} P}{\sum_{t-1}^{t} P + \sum_{t-1}^{t} M}, \text{and} \tag{2.7} $$

$$ {}_{t-1}^{t}\mathrm{R}_{\mathrm{melt}} = 1 - {}_{t-1}^{t}R_{\mathrm{precip}}, \tag{2.8} $$

where t and $t-1$ are the observation time and previous observation time, respectively. The relative contribution is determined by meteorological variables defined by MicroMet. Once the snow process is known, a precipitation or melt factor is calculated in order to correct the initial SnowModel precipitation and melt needed to match the SWE observations. In the simplest form, the precipitation correction factor is

$$ {}_{t-1}^{t}\mathrm{P}_{\mathrm{fact}} = \frac{\mathrm{SWE}_{obs}^{t} - \mathrm{SWE}_{obs}^{t-1}}{\mathrm{SWE}_{mod}^{t} - \mathrm{SWE}_{mod}^{t-1}} \tag{2.9} $$

Assuming,

$$ \sum_{t-1}^{t} P \approx \mathrm{SWE}_{mod}^{t} - \mathrm{SWE}_{mod}^{t-1}, \tag{2.10} $$

and by adding and subtracting $\frac{\sum_{t-1}^{t} P}{\sum_{t-1}^{t} P}$ from the right side of Equation 2.10 and rearranging, Equation 2.10 becomes:

$$ {}_{t-1}^{t}\mathrm{P}_{\mathrm{fact}} = 1 + \frac{(\mathrm{SWE}_{obs}^{t} - \mathrm{SWE}_{mod}^{t}) - (\mathrm{SWE}_{obs}^{t-1} - \mathrm{SWE}_{mod}^{t-1})}{\sum_{t-1}^{t} P} \tag{2.11} $$

A similar process is done for the melt factor and is given by:

$$ {}_{t-1}^{t}\mathrm{M}_{\mathrm{fact}} = 1 - \frac{(\mathrm{SWE}_{obs}^{t} - \mathrm{SWE}_{mod}^{t}) - (\mathrm{SWE}_{obs}^{t-1} - \mathrm{SWE}_{mod}^{t-1})}{\sum_{t-1}^{t} M}. \tag{2.12} $$

For this study, SnowAssim is the most important component of SnowModel, as it allows remotely sensed and in-situ SWE datasets to be coupled to the snow evolution properties needed to consistently compare the initial snowfall and subsequent SWE. This allows for the comparison between the observed AMSR-E snowfall and the snowfall needed to match the observed AMSR-E SWE while taking into account the snow evolution that must be considered.

2.5 MERRA-2 Precipitation

Because precipitation is the main driver of snow cover, an overview of the production of precipitation in MERRA-2 is necessary. MERRA-2 includes improved assimilation techniques to update the Goddard Earth Observing System version 5 (GEOS5) general circulation model. It includes important precipitation parameterizations made in the MERRA-Land product that have shown to improve precipitation dynamics (Reichle et al. 2011). These include the areal fraction of interception by vegetation that captures large scale and convective precipitation as well as changes to the minimum SWE depth in snow covered areas that improves the modeled albedo.

MERRA-2 contains two types of precipitation estimates: the precipitation produced by the AGCM (M2AGCM) and the corrected land-surface precipitation (M2CORR). Two NOAA Climate Prediction Center (CPC) precipitation products are used to produce the M2CORR product: CPC Unified Gauge-Based Analysis of Global Daily Precipitation (CPCU) and CPC Merged Analysis of Precipitation (CMAP). These two datasets are used to correct M2AGCM in four distinct regimes. The precipitation regimes most relevant to this study are summarized in Table 2.2. Neither M2AGCM nor the observational correction datasets used to produce M2CORR contain AMSR-E precipitation estimates.

Table 2.2. MERRA-2 Precipitation Correction Regimes.

Land Region	**Observations (temporal/spatial resolution)**	**Correction**
Low and Mid latitude ($<42.5^\circ$)	CPCU (daily/0.5°)	Full correction to observations
Mid and High latitude (42.5° - 62.5°)	CPCU (daily/0.5°)	Linear tapering between full and no correction
High latitude ($>62.5^\circ$)	None	No correction

2.6 Canadian Meteorlogical Centre Snow Analysis

The Canadian Meteorological Centre (CMC) Snow Analysis is an operational product consisting of daily snow depth analysis as well as monthly averages of snow depth and SWE for the Northern Hemisphere. The snow depth output is produced using daily in-situ snow depth observations that are optimally interpolated onto a first-guess snow depth field estimated by a simple snow

model (Brasnett 1999). The simple snow model does not account for all types of physical snow processes such as sublimation, condensation, wind-driven snow, and snowpack evolution. The contribution from the station observation to the background snow field decreases with distance from the station. The model is driven by meteorological data from the CMC Global Environmental Multiscale (GEM) forecast model and in-situ snow depth data is collected from surface synop stations, meteorological aerodrome reports (METAR) stations, and special aviation reports from the WMO. Despite the limitations of the simple snow model used in the CMC snow analysis, it is one of the few long-term, observationally constrained snow depth datasets that exist. It is widely used in snow depth comparison studies and has been described as the best-available observational snow dataset for the Northern Hemisphere (Toure et al. 2016).

2.7 Snow Data Assimilation System

The Snow Data Assimilation System (SNODAS) is a snow modeling and data assimilation system developed and operated by the National Operational Hydrologic Remote Sensing Center (NOHRSC). Its goal is to provide the best possible estimates of snow variables for the Conterminous United States (CONUS) using a physically consistent framework outlined in Carroll et al. (2001). SNODAS includes models to ingest and downscale meteorological output from the Rapid Update Cycle (RUC2) weather model, perform snow energy and mass balance calculation from a physically based snow model, and assimilate snow extent and SWE observations from satellites, airborne, and in-situ platforms. Each day, an analyst manually determines if observations should be used to update the SWE state. Snow state variables are solved for at three separate snow layers using output from the snow thermal model SNTHERM.89 (Jordan 1990). Total snowpack SWE, snow depth, snow melt runoff, snowpack sublimation, precipitation, and snowpack temperature are output on a 1km grid at daily timescales.

CHAPTER 3

Results from SnowModel Assimilation

3.1 Experimental Setup

In order to compare snowfall with SWE in a consistent way, a model was used to evolve the snowpack over time. Because of the availability of the SnowModel routines described previously, we assimilated AMSR-E, CMC, and SNODAS SWE into SnowModel (through the SnowAssim routine), which in turn adjusts the snowfall to be consistent with the observed SWE and meteorological forcing. The procedure was performed for each SWE product to find the appropriate snowfall amount to match the observed SWE from AMSR-E, CMC, and SNODAS. The inferred snowfall was then compared directly to the observed AMSR-E snowfall product to assess the magnitude and regions of consistency and inconsistency. All the results focused on the average accumulated snowfall and SWE for February for all simulation years with a focus on six regions shown in Figure 3.1. These regions included the Western CONUS, the Great Plains, the Eastern CONUS, Canada, Eastern Europe, and Siberia. February was chosen to eliminate complications of AMSR-E retrieving SWE during snowmelt. Figure 3.1 also includes SNOTEL, WMO station data, and radar data to show the spatial variability of global snow observations.

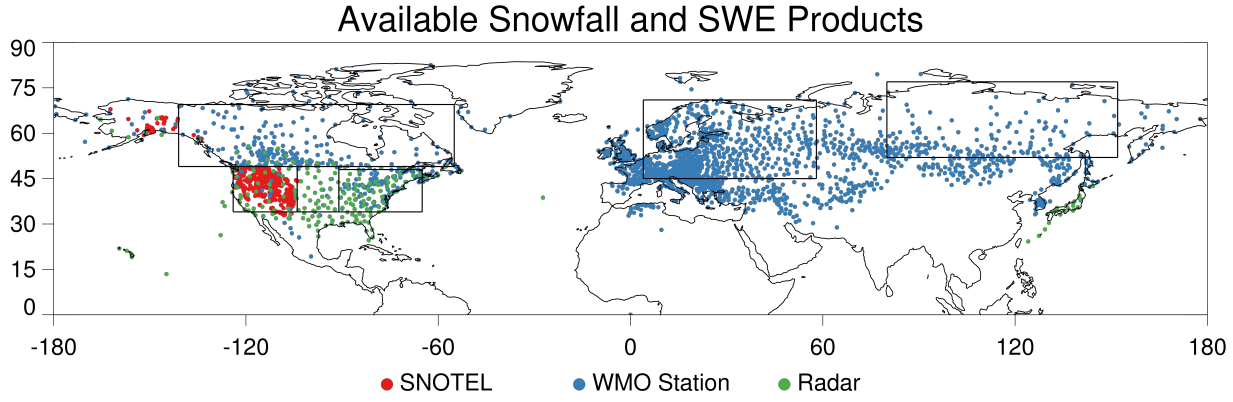

Fig. 3.1. Available snowfall and SWE products including SNOTEL, WMO station data, and radar (NEXRAD, Canadian Weather Radar, and Japanese Radar Network). Available data is not exclusive to these products and is shown to present general location of a few available products.

All available SWE data for AMSR-E, CMC, and SNODAS were obtained for the simulation period of July 2003 to June 2011. Each dataset has unique map projections, horizontal resolutions, and temporal resolutions that were converted to a common projection and resolution to simplify comparisons. The nominal spatial and temporal resolutions of each dataset are summarized in Table 3.1.

Table 3.1. Nominal resolution of SWE datasets.

Product	**Availaibility**	**Grid Size**	**Projection**	**Temporal Resolution**
AMSR-E	2003-2011	25km	EASE 2.0	Daily, Pentad, Monthly
CMC	1998-Present	24km	Polar Stereographic	Monthly
SNODAS	2003-Present	1km	Equirectangular	Daily

The Northern Hemisphere 25km Equal-Area Scalable Earth (EASE) grid was chosen for this study because it minimizes the amount of distortion at the North Pole, which is a useful focal point for Northern Hemisphere snow studies. The nominal EASE-grid was cropped near the equator to exclude gridpoints that have a low probability of snow cover. Data was resampled to a common grid using the Geospatial Data Abstraction Library (GDAL). Observed AMSR-E snowfall was also obtained for the same period and resampled to the custom EASE-grid. Because we are concerned about regional biases in the snow products, all SWE and snowfall data were averaged to a monthly value at every gridpoint. To better assess snowfall against SWE, accumulated snowfall for each simulation year was used. A simulation year is defined from July of one year to June of the next year (e.g. July 2004 - June 2005).

SnowModel meteorological forcing data was provided by MERRA-2. MERRA-2 surface pressure, 10m air temperature, 10m wind, 10m specific humidity, and bias corrected total precipitation (M2CORR) were downloaded for the simulation period. Forcing variables were resampled to the custom EASE-grid, converted to the correct MicroMet variables, and correctly formatted to be ingested into SnowModel.

SnowModel simulates snow evolution using consistent meteorological forcing. SnowModel was run for the simulation period on the custom EASE-grid. The model was run at 3-hour timesteps, which is sufficient to capture the diurnal cycle of snow evolution. At each timestep,

snow is evolved following the SnowModel steps previously described. For this study, the sub-model SnowTran was not employed, and snow transport processes were not simulated. Given the regional nature of this study, this is not expected to impact the results. Elevation and vegetation data were provided by the United States Geological Survey (USGS) Global Multi-resolution Terrain Elevation Data (GMTED2010) and NASA's GlobCover, respectively.

SWE from AMSR-E, CMC, and SNODAS were assimilated into SnowAssim on the 15th day of October, December, February, and April to provide constraints throughout the snowpack accumulation and ablation periods. An example of the assimilation processes is shown in Figure 3.2. It shows the SNODAS SWE and corresponding accumulated inferred SNODAS snowfall and MERRA-2 snowfall for the Western CONUS during the winter of 2010-2011. SnowAssim increases the MERRA-2 precipitation in order to match the observed SNODAS SWE.

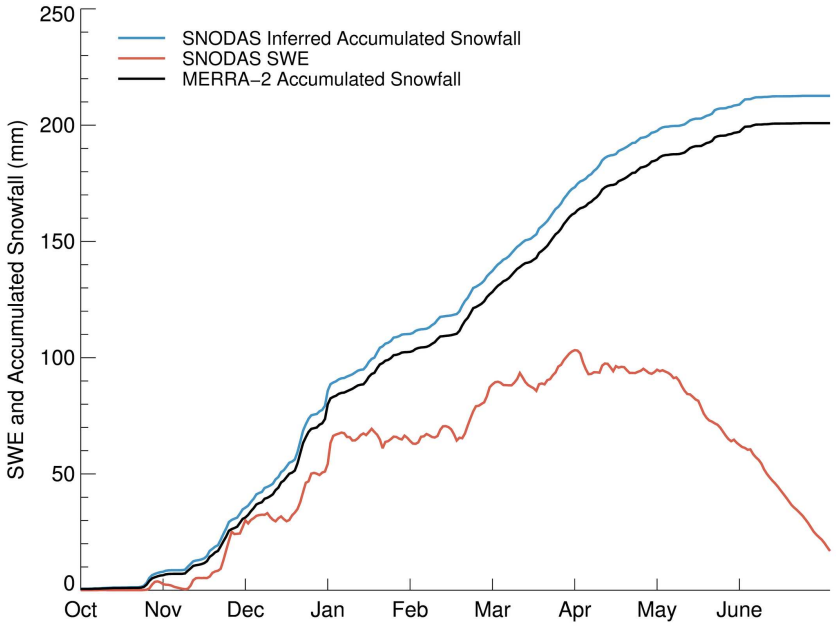

Fig. 3.2. SNODAS SWE for the Western CONUS from October 2010 to June 2011 with the corresponding accumulated inferred SNODAS snowfall and accumulated MERRA-2 snowfall.

It is important to note the inferred snowfall of AMSR-E, CMC, and SNODAS is initially MERRA-2 snowfall that is scaled following the SWE observations. Other than the constrained

snowfall, the forcing data remains constant for each simulation. A total of three model simulations with assimilation were run: one each for AMSR-E, CMC, and SNODAS. Table 3.2 shows the global bias and correlation between the SWE datasets and MERRA-2 before assimilation as well as the SWE datasets and corrected MERRA-2 SWE after assimilation. Table 3.2 provides evidence the assimilation process works nominally.

Table 3.2. Biases (correlation) of average February SWE for assimilation using SnowAssim. Computations use gridcells that consist of SWE for both datasets.

	AMSR-E	**CMC**	**SNODAS**
Before	-29.69 (0.19)	-9.82 (0.55)	-1.29 (0.82)
After	-2.55 (0.95)	1.61 (0.96)	0.69 (0.99)

3.2 AMSR-E Snowfall

The spatial patterns of accumulated snowfall are generally consistent for MERRA-2, inferred CMC, and inferred SNODAS, but show a different pattern for AMSR-E (Figure 3.3). The expected regions of large snowfall amounts at high latitudes and high elevation are captured by the modeled datasets. AMSR-E observes significantly less snowfall than is indicated by the modeled datasets in a majority of regions, and is especially pronounced at high elevations and high latitudes. The global accumulated snowfall bias between AMSR-E and the inferred snowfall datasets exceeds -54 mm, or -75%. The highest snowfall amounts observed by AMSR-E are in the Pacific Northwest, Eastern North America, and Eastern Europe. For the remainder of the thesis, it is important to note that the CMC and SNODAS snowfall is the inferred snowfall using the CMC and SNODAS SWE products and SnowAssim.

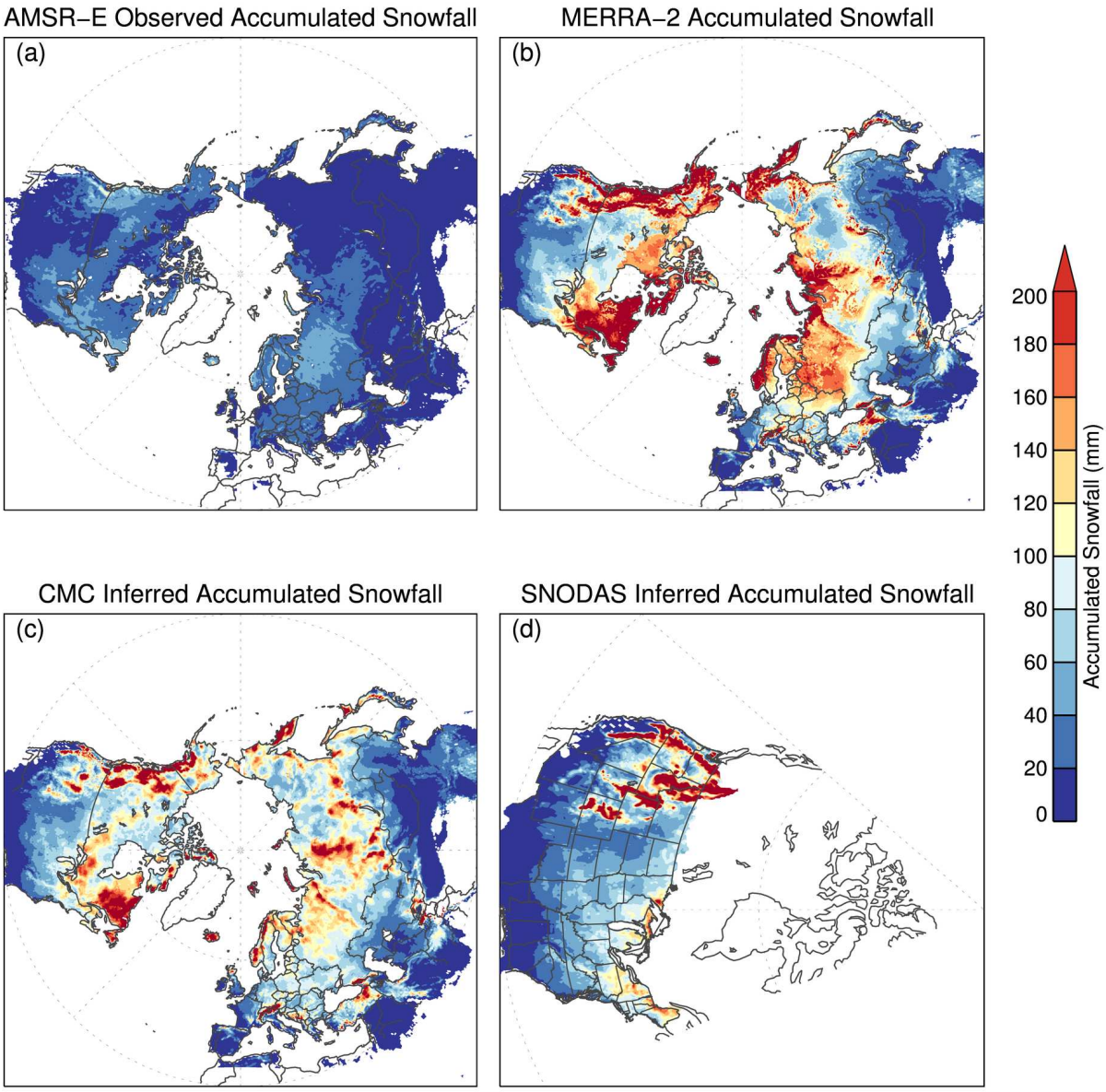

Fig. 3.3. (a) AMSR-E observed accumulated snowfall, (b) MERRA-2 accumulated snowfall, (c) CMC inferred accumulated snowfall, (d) SNODAS inferred accumulated snowfall. Snowfall is accumulated from the period of July-February and amounts are averaged for 8 simulation years 2003-2011.

The snowfall bias between MERRA-2 and CMC is shown in Figure 3.4. CMC underestimates snowfall compared to MERRA-2 at high latitudes above 60°N. Compared to MERRA-2, CMC underestimates accumulated snowfall in Eastern Europe with an average bias of -44%. Regions of large underestimation also occur in the mountainous regions of the Western CONUS and the Eastern CONUS with average biases of -22% and -21%, respectively. CMC produces regions of higher snowfall amounts in central Canada extending into the Great Lakes, but on average underestimates snowfall by 27%. In Canada, regions of underestimation are at high latitudes, the mountains of the Pacific coast, Quebec, and Newfoundland. The CMC SWE product has known issues at high latitudes due to the lack of WMO gauge observations (Figure 3.1). In areas with few gauges, the SWE product relies on the output from the simple snow model. There is no systematic bias observed for regions with and without a high density of gauges. For example, the Western CONUS and Eastern Europe both produce less snowfall than MERRA-2, but Eastern Europe contains significantly more gauges. The regions of overestimation generally have good gauge coverage. Other than high latitudes, there is little evidence in literature of known biases in the CMC product and therefore it is difficult to determine the underlying cause of the differences.

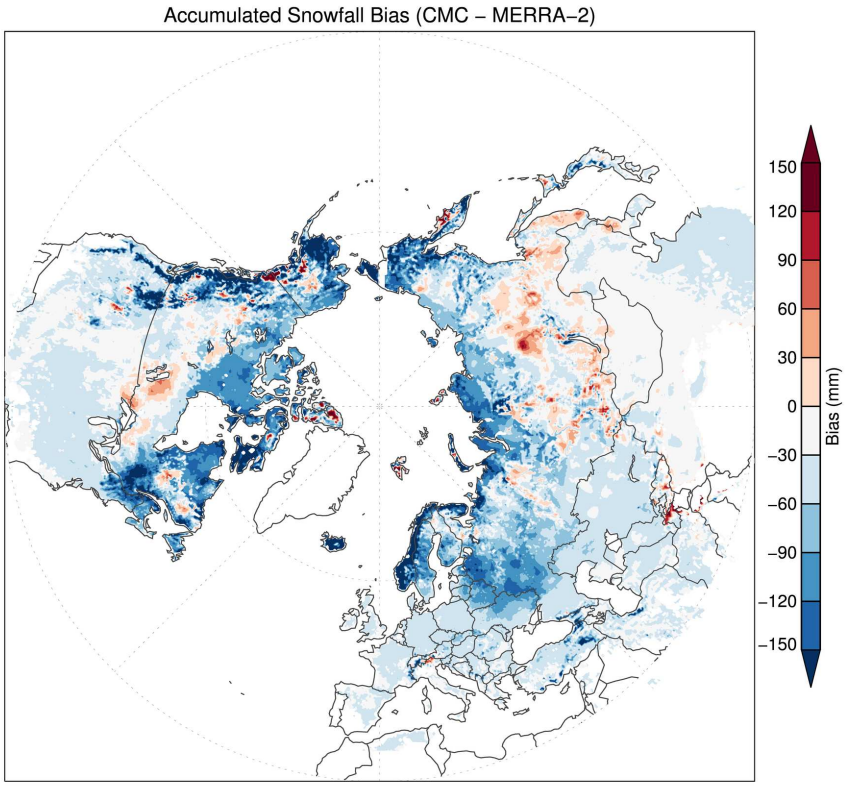

Fig. 3.4. Accumulated snowfall bias between inferred CMC and MERRA-2. Snowfall is accumulated from the period of July-February and amounts are averaged for 8 simulation years 2003-2011.

Snowfall biases between MERRA-2 and SNODAS show similarities to MERRA-2 and CMC biases in the Great Plains and the Eastern CONUS, but differences exist in the Western CONUS (Figure 3.5). SNODAS underestimates snowfall compared to MERRA-2 in the Eastern CONUS by an average of -17%, which is comparable to the MERRA-2 and CMC biases for this region. The average overestimation by SNODAS snowfall by 9% in the Great Plains is also similar to the MERRA-2 and CMC bias in the Great Plains. Biases in these regions have similar spatial patterns and suggest MERRA-2 overestimates snowfall in the Eastern CONUS and underestimates snowfall in the Great Plains. In the Western CONUS, SNODAS produces more snowfall in the central Rocky Mountains and less snowfall in the Cascade Mountains.

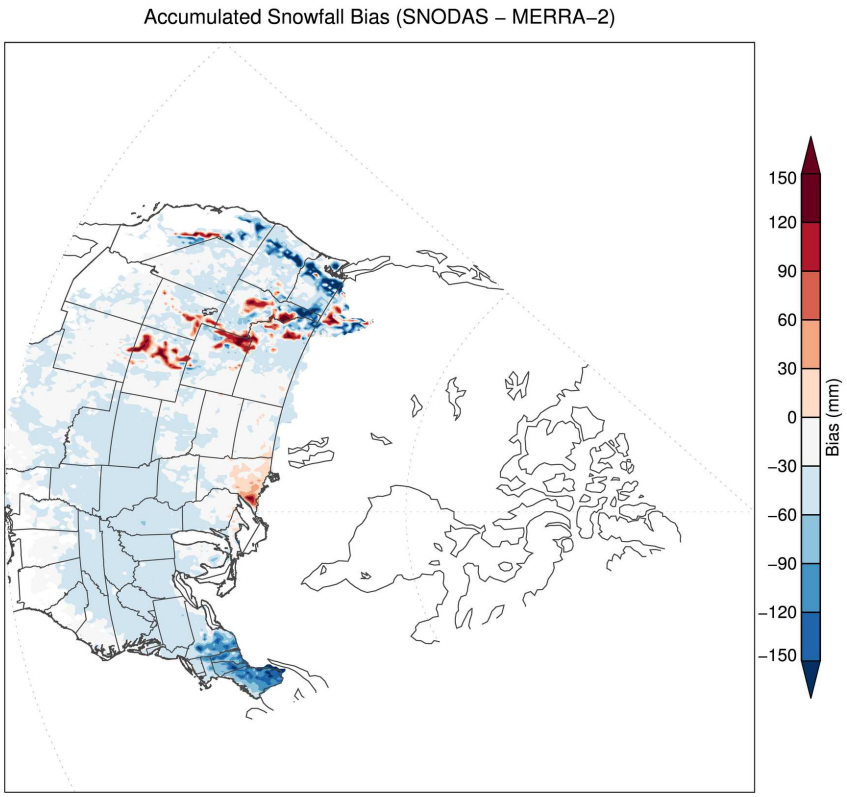

Fig. 3.5. Accumulated snowfall bias between inferred SNODAS and MERRA-2. Snowfall is accumulated from the period of July-February and amounts are averaged for 8 simulation years 2003-2011.

As expected from previous analysis, the biases are on average near 0% for the Great Plains and the Eastern CONUS between CMC and SNODAS (Figure 3.6). The average bias of 31% in the Western CONUS is the highest between all combinations of datasets. SNODAS produces more snowfall in the Rocky, Sierra, and Cascade Mountains. Both the CMC and SNODAS product use an initial snow model that is nudged towards gauge observations. However, the SNODAS snow model is more complex and accounts for more physical processes that affect snow evolution. Additionally, the number of gauges used in the CONUS domain is significantly higher for SNODAS than CMC, which allows SNODAS to better match gauge data at a higher spatial resolution, especially in the mountains. In the Canadian Rocky Mountains, SNODAS produces an average of 40% more snowfall than CMC.

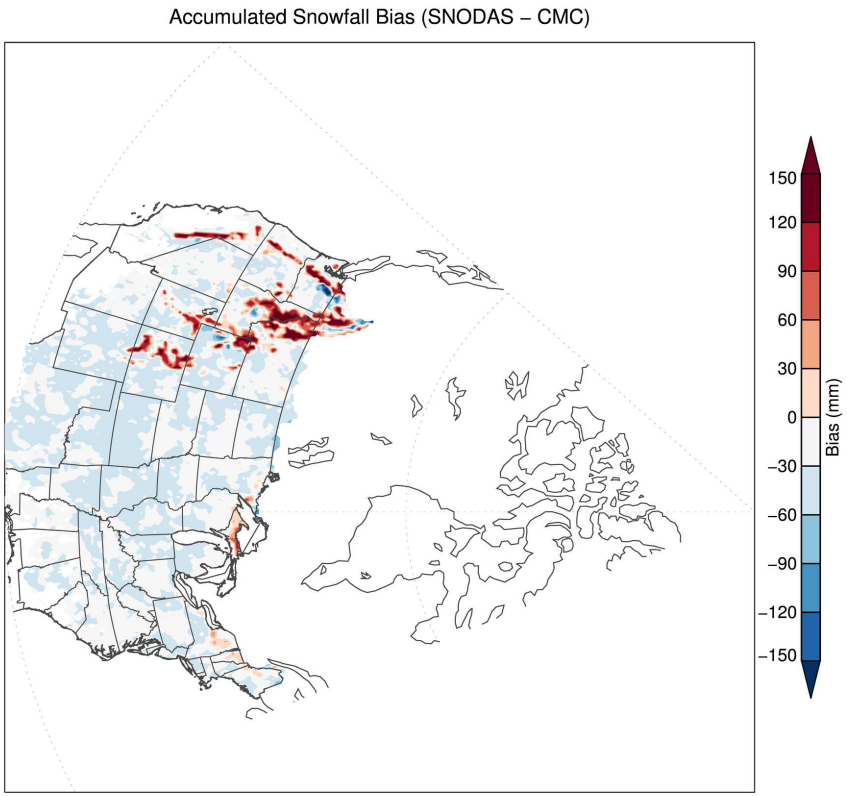

Fig. 3.6. Accumulated snowfall bias between inferred SNODAS and inferred CMC. Snowfall is accumulated from the period of July-February and amounts are averaged for 8 simulation years 2003-2011.

To assess the validity AMSR-E snowfall products without having any absolute truths, it is useful to define a best-guess snowfall product that is constructed from MERRA-2, CMC, and SNODAS and represents a merged product of each dataset based on the above discussion. The best-guess snowfall product is determined by taking into account the biases observed between the snowfall datasets and is formulated by: 1) MERRA-2 snowfall above 60°N, 2) average MERRA-2 and CMC snowfall for the remainder of the domain besides CONUS, 3) average CMC and SNODAS snowfall for the Great Plains and the Eastern CONUS, and 4) average MERRA-2 and SNODAS snowfall for the Western CONUS. The MERRA-2 product is used at high latitudes because the CMC product is known to underestimate snow at high latitudes. For the rest of the global domain excluding CONUS, an average between the MERRA-2 and CMC products is used

because they are the only two global products used to create the best-guess product. In the Great Plains and Eastern CONUS, CMC and SNODAS are used because it is shown the two products have near-zero biases in these regions. In the Western CONUS, CMC underestimates snowfall, and thus, MERRA-2 and SNODAS are used. Essentially the best-guess snowfall product is created by a majority agreement between the products. Figure 3.7 indicates AMSR-E does not observe sufficient snowfall globally to agree with the best-guess product anywhere.

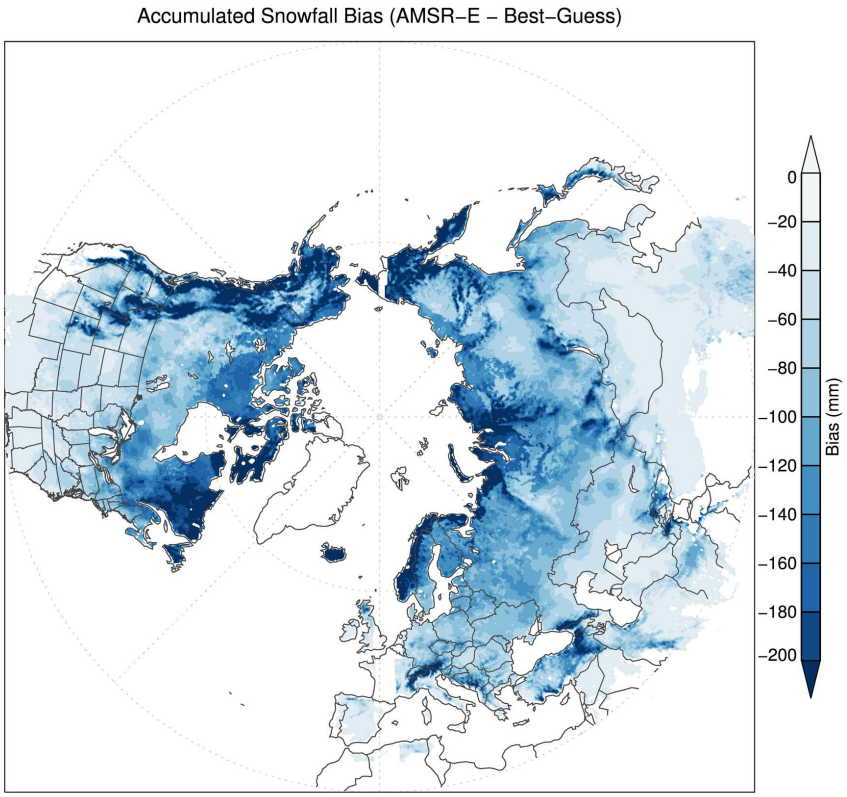

Fig. 3.7. Accumulated snowfall bias between the observed AMSR-E and Best-Guess products. Snowfall is accumulated from the period of July-February and amounts are averaged for 8 simulation years 2003-2011.

Note the change in color bar compared to previous bias maps. All regions indicate a negative bias of AMSR-E snowfall. The Great Plains and the Eastern CONUS have the smallest biases near -60%. While AMSR-E does observe higher amounts of snowfall in the Western CONUS and Eastern Europe, the biases are still -75% and -80% compared to the best-guess snowfall dataset,

respectively. AMSR-E underestimates snowfall by an average of -84% across the Canadian region. In Canada, the underestimations are concentrated mainly in high latitude regions and the mountainous region along the Pacific coast. Siberia has the largest different with a bias of -88%. Given the snowfall biases between AMSR-E and the other datasets, AMSR-E snowfall is not sufficient to match any of the other datasets. However, it is informative to also analyze the observed AMSR-E SWE to see how it compares with the other SWE products to assess the spatial bias patterns between the AMSR-E snowfall and SWE products.

3.3 AMSR-E SWE

To assess the spatial pattern in SWE between the datasets, Figure 3.8 shows the average February SWE for all the datasets used. It is important to note the MERRA-2 SWE, is SnowModel SWE driven by MERRA-2 reanalysis. Generally, the spatial patterns of SWE are similar to snowfall patterns with high amounts of SWE in mountainous regions and at high latitudes. Again, the most dissimilar product is AMSR-E, which has known difficulties in different meteorological, orographic, and vegetation regimes. Known difficulties include, but are not exclusive to, overestimation of SWE in Siberia, underestimation in mountainous regions such as the Western CONUS, and underestimation in forested regions such as the Northeast United States.

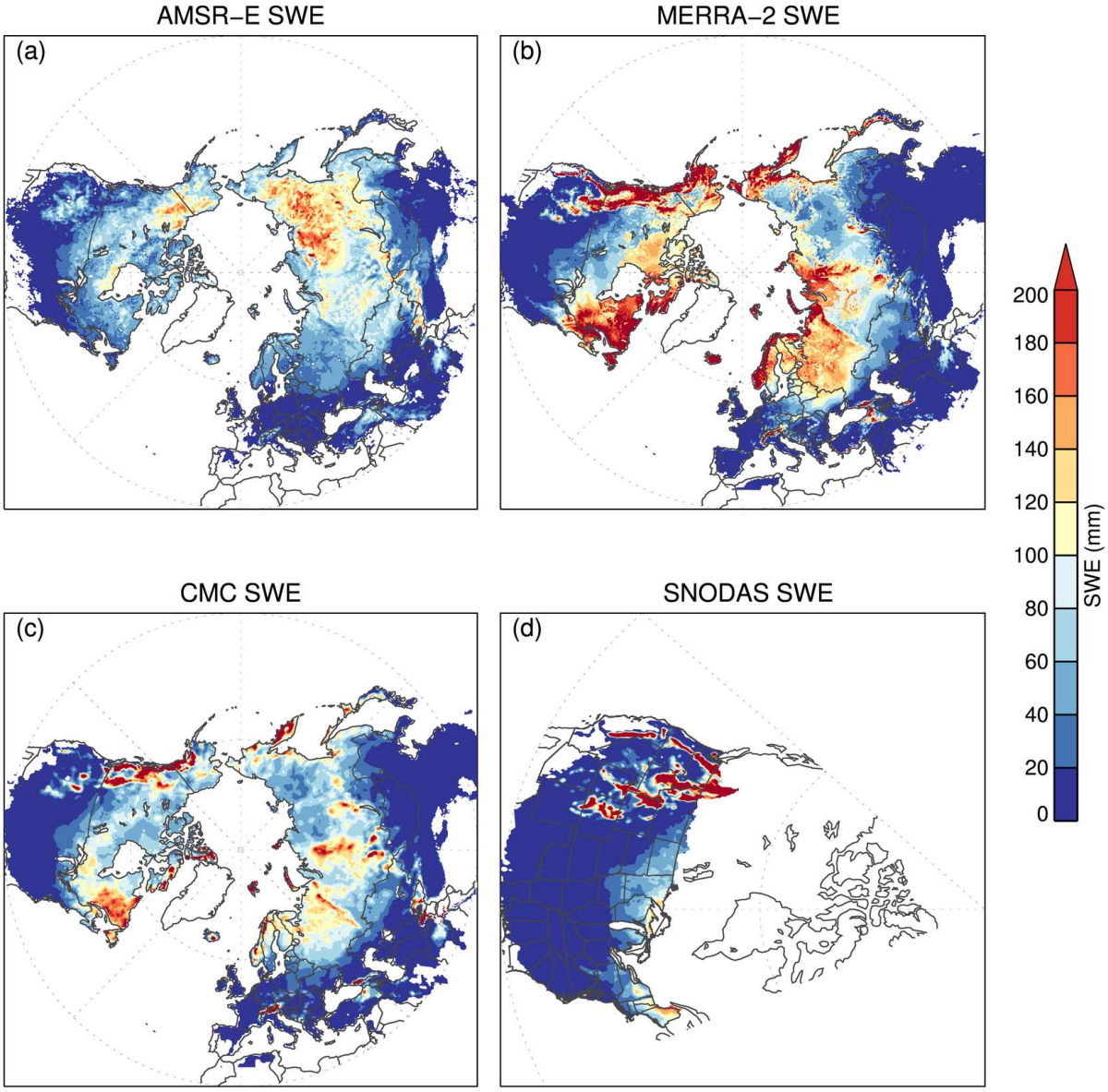

Fig. 3.8. (a) AMSR-E observed SWE, (b) MERRA-2 SWE, (c) CMC SWE, (d) SNODAS SWE. SWE is averaged for 8 simulation years 2003-2011 during the month of February.

The AMSR-E SWE product is compared against a best-guess SWE product using the same metrics as those used to produce the best-guess AMSR-E snowfall product. The best-guess SWE product is formulated by: 1) MERRA-2 SWE above 60°N, 2) average MERRA-2 and CMC SWE for the rest of the domain besides CONUS, 3) average CMC and SNODAS SWE for the Great Plains and the Eastern CONUS, and 4) average MERRA-2 and SNODAS SWE for the Western

CONUS. Figure 3.9 shows a significantly different SWE bias pattern compared to the AMSR-E snowfall bias pattern (Figure 3.7).

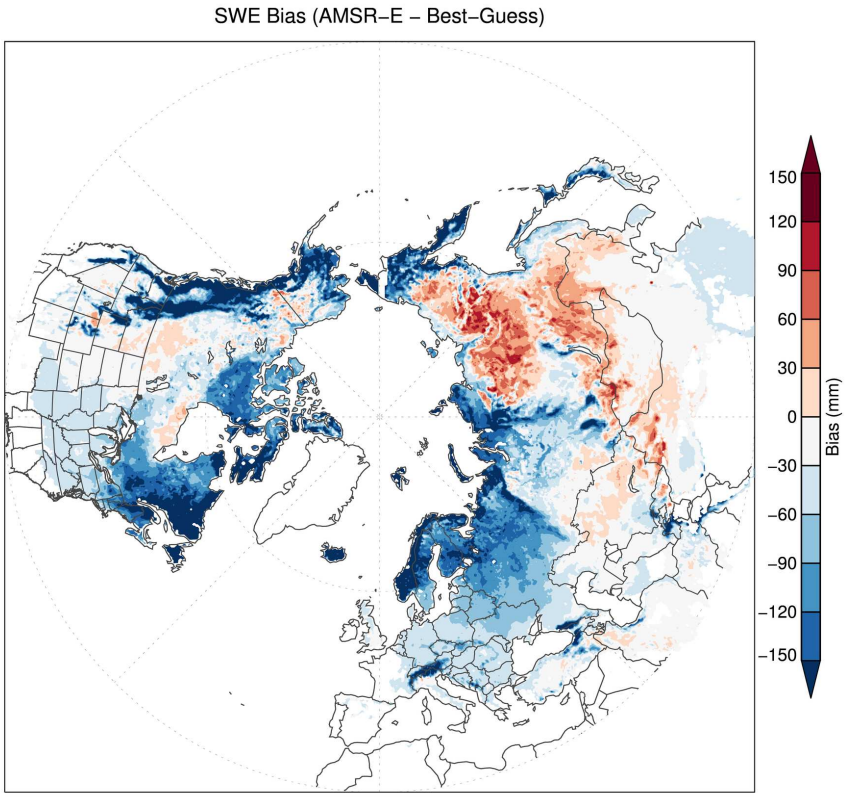

Fig. 3.9. SWE bias between the observed AMSR-E and Best-Guess products. SWE is averaged for 8 simulation years 2003-2011 during the month of February.

Unlike the snowfall bias which was entirely negative, the SWE bias contains pronounced biases that are both positive and negative. The Siberia and Great Plains regions produce more SWE compared to the best-guess product on average by 18%. Siberia is dominated by large positive and negative biases whereas there is a relatively smooth bias across the Great Plains. AMSR-E underestimates SWE in mountainous regions of the Western CONUS by 56%. The underestimation in mountainous regions is also observed in the northern Rocky Mountains, Scandinavia, the Alps, and the Ural Mountains. Interestingly, Eastern Europe is a large region of underestimation (-69%) by AMSR-E, which has not been previously identified in the literature. AMSR-E underestimates

SWE in the Eastern CONUS region on average by -67%, but this is mainly isolated to forested regions in the far northeast United States. AMSR-E observes higher amounts of SWE compared to the best-guess product near the Canada-Alaska border, central Canada, and south of the Hudson Bay. Elsewhere in Canada, AMSR-E significantly underestimates SWE by an average of 56%. The regions of underestimation are located in regions of greater than 200 mm of SWE in the best-guess SWE product, which can cause saturation of the microwave signal.

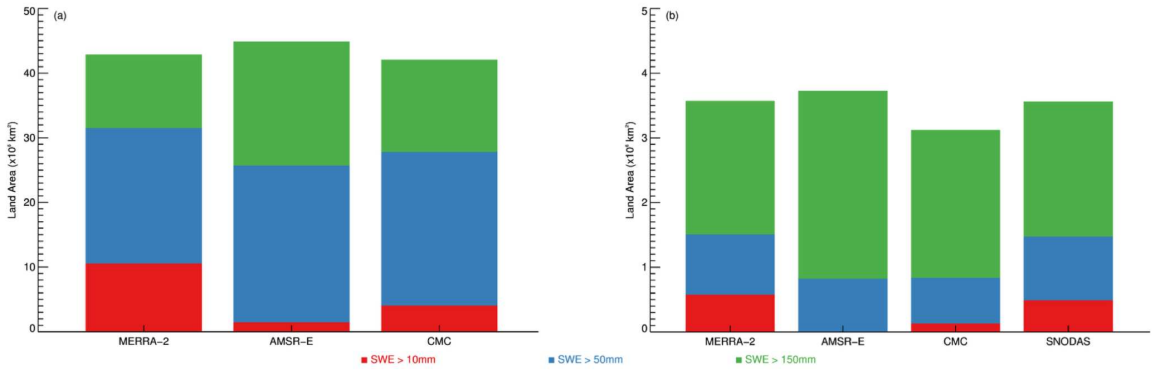

Fig. 3.10. Snow-cover land area for average February SWE based on SWE $>$ 10, 50, 150 mm for (a) global SWE products and (b) CONUS SWE products.

The AMSR-E SWE algorithm detects more land covered by SWE than MERRA-2, CMC, and SNODAS (Figure 3.10). AMSR-E produces 9.1 x 10^6 km^2 (151%) and 2.6 x 10^6 km^2 (94%) less land covered by 150 mm of SWE compared to MERRA-2 and CMC, respectively. Generally, the land covered by more than 150 mm of SWE in the AMSR-E product does not correspond to similar locations in MERRA-2 and CMC. AMSR-E estimates more land cover for SWE amounts between 50 mm and 150 mm by up to 3.3 x 10^6 km^2 (14%). Furthermore, AMSR-E estimates up to 7.8 x 10^6 km^2 (51%) more land covered by SWE amounts between 10 mm and 50 mm. MERRA-2 estimates the least amount of land cover for all categories except for land covered by more than 150 mm of SWE.

In the CONUS, MERRA-2 and SNODAS produce similar estimates of total land covered by SWE as well as the amount of land covered by SWE for each category. CMC estimates 0.44 x 10^6 km^2 (126%) less land cover than MERRA-2 for areas with more than 150 mm of SWE. This difference arises because CMC does not produce high amounts of SWE throughout the mountainous

regions of the Western CONUS. AMSR-E does not produce any regions of SWE cover for more than 150 mm of SWE, but produces the largest total land covered by SWE. The total amount of SWE cover for AMSR-E is dominated by SWE amounts between 10 mm and 50 mm.

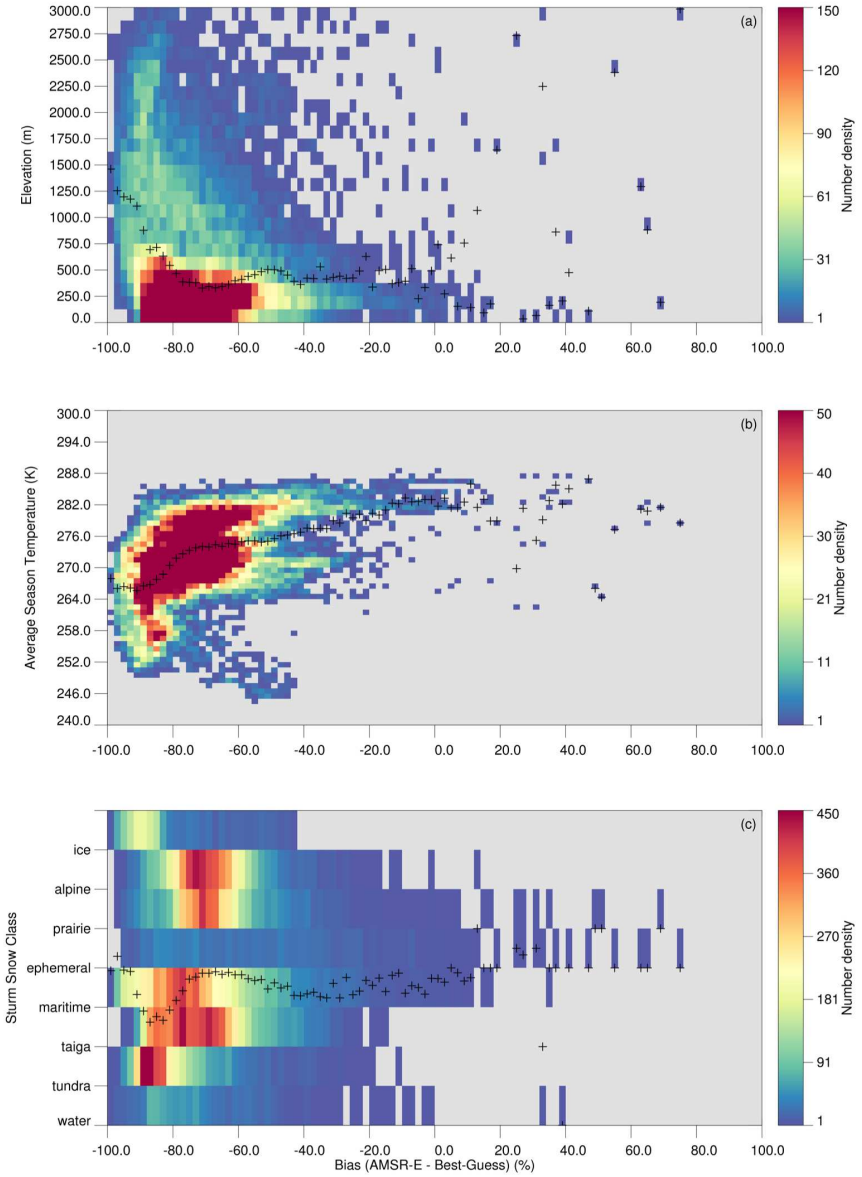

Fig. 3.11. Percent bias of the AMSR-E observed accumulated snowfall and best-guess accumulated snowfall as a function of (a) SnowModel elevation, (b) SnowModel surface temperature, and (c) Sturm et al. (1995) snow class. Snowfall is accumulated from the period of July-February and amounts are averaged for 8 simulation years 2003-2011.

3.4 AMSR-E Snowfall and SWE Bias Analysis

Figure 3.11 shows the snowfall biases as a function of temperature, snow class, and elevation. Temperature is chosen to be the average temperature for the period between July and February. Snowfall biases less than -60% have an average temperature of less than 270K. Biases tend to become less negative as temperature increases. AMSR-E is biased low in excess of 80% are largely represented by tundra and taiga snow classes, which comprise the majority of the surface snow class above 50°N. Tundra and taiga snow classes exhibit the lowest temperatures, low-to-moderate ($<$ 1200 mm) snowfall, and large snow grains, suggesting GPROF has the greatest difficulty in retrieving snowfall in cold, high-latitude regimes. Maritime and alpine snow regimes that make up the highest amounts of snowfall are generally underestimated between -80% and -60%. Snowfall bias as a function of elevation shows a peak in biases at high elevation with biases decreasing with decreasing elevation.

Figure 3.12 shows the SWE biases as a function of temperature, snow class, and elevation. Unlike AMSR-E snowfall biases, there is not a large dependency on surface temperature for SWE biases. Warmer temperatures with large negative biases are contained to the south and central Rocky Mountains, the Pacific Northwest, and much of Eastern Europe. Large negative biases with cold temperatures are at high latitude regions. Many gridpoints that exhibit biases greater than 100% are observed in a wide temperature range from 254K-274K. SWE biases are dominated by the tundra and taiga snow class with a large frequency of biases greater than 100% limited to these two classes. Maritime and alpine biases are largely restricted to underestimation by AMSR-E because of the saturation effect caused by microwave interactions with deep snowpack. Tedesco and Narvekar (2010) showed the saturation effect for the current SWE algorithm occurs around 600 mm. The largest negative SWE biases have an average elevation near 1000m, with little dependency on elevation for the rest of the biases.

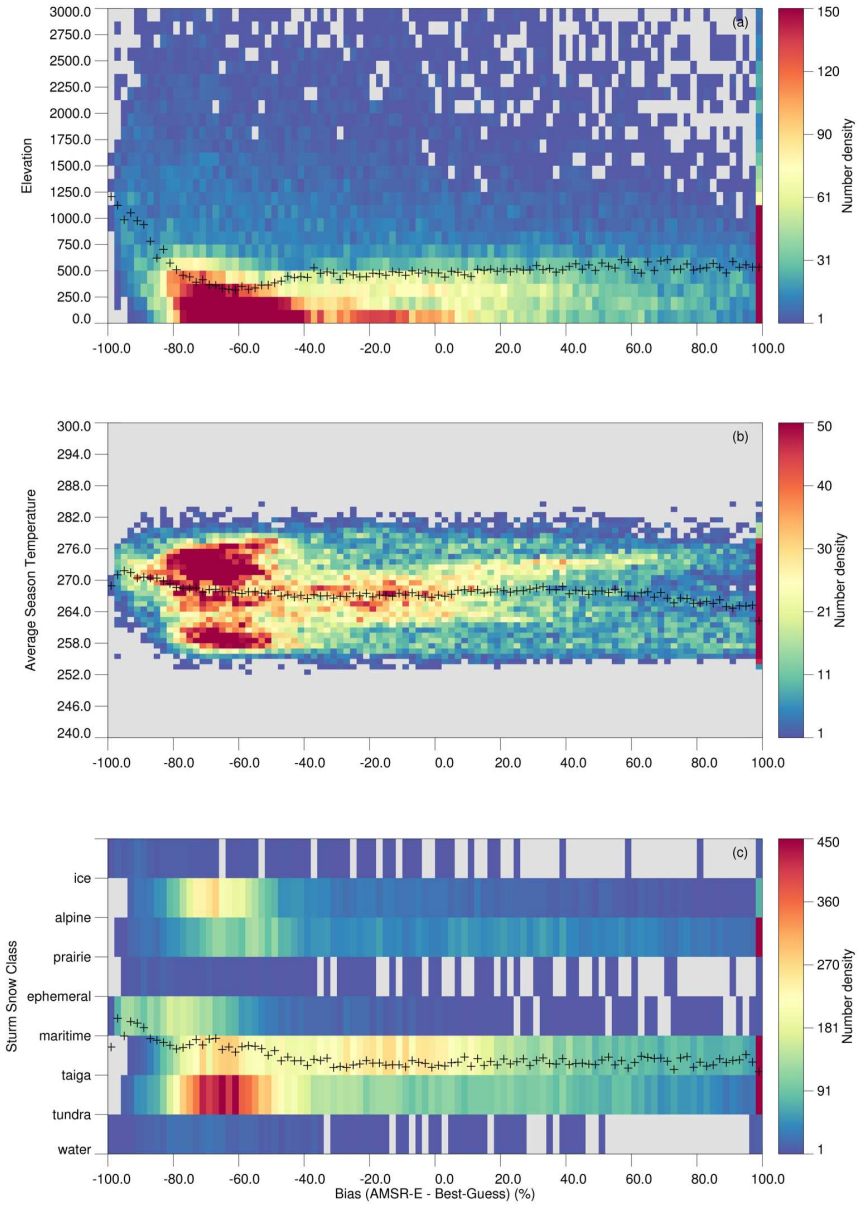

Fig. 3.12. Percent bias of the AMSR-E observed SWE and best-guess SWE as a function of (a) SnowModel elevation, (b) SnowModel surface temperature, and (c) Sturm et al. (1995) snow class. SWE is averaged for 8 simulation years 2003-2011 during the month of February.

3.5 Consistency in the AMSR-E Snow Products

The consistency between the observed snowfall and the required snowfall is shown in Figure 3.13. This comparison allows consistency checks in the snow products because of the assimilation of AMSR-E into SnowModel. While the AMSR-E snow products, particularly based upon

the findings of this study, would hardly be expected to show closure, some regions show some consistency. To close the snow budget, regions within 25% bias are considered to achieve closure and include parts of the Western CONUS, the Great Plains, the Eastern CONUS, and Eastern Europe. Other than the Appalachian Mountains, all the other regions are shown to underestimate SWE on average. Western CONUS appears to close largely because both the snowfall and SWE appear to be significantly underestimated. Consequently, although there is consistency between the AMSR-E products, the required snowfall amounts are not sufficient to produce the best-guess SWE product. Snowfall and inferred snowfall differ by more than a factor of 10 in Siberia, which is an area of concern for the AMSR-E SWE product. AMSR-E does not observe adequate amounts of snowfall in this region compared to the best-guess snowfall, but the biases in snowfall are significantly lower than the closure biases. A similar overestimation occurs near the Canada-Alaska border and south of the Hudson Bay. Derksen and MacKay (2006) identified this region of high passive microwave observations of SWE to be consistent with ground data from field campaigns.

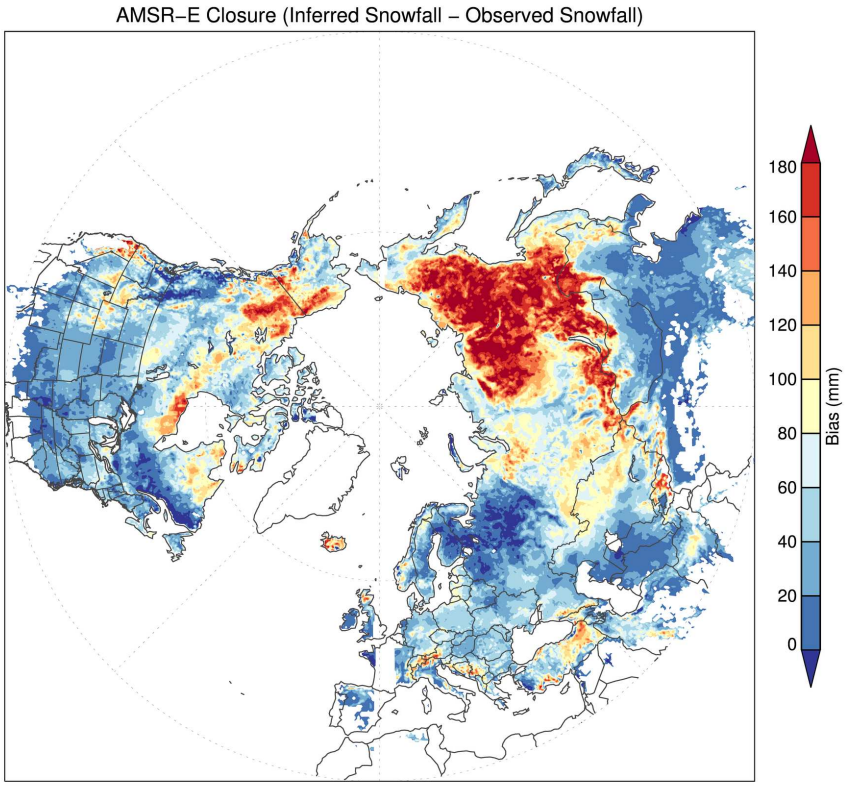

Fig. 3.13. Closure in AMSR-E snow products shown as inferred AMSR-E snowfall minus observed AMSR-E snowfall. Snowfall is accumulated from the period of July-February and amounts are averaged for 8 simulation years 2003-2011.

CHAPTER 4

Discussion and Outlook

Snow was shown to be difficult to accurately model or observe. Satellite platforms produce global snowfall and SWE observations at high temporal resolution in regions where in-situ data is not available. This study examines the consistency, to first order, between AMSR-E snowfall and SWE observations using a snow modeling system (SnowModel) to provide the ability to consistently compare snowfall and SWE. The goal of this study is to not validate the snowfall and SWE products, but rather identify deficiencies in both products that can be information for future improvement.

It has been shown AMSR-E underestimates snowfall globally with larger underestimation confined to cold regions, high-latitudes, and mountains. AMSR-E SWE exhibits a different bias pattern that does not show a strong dependency on temperature and elevation, but rather on snow class. AMSR-E overestimates total snow covered area and has difficulty accurately producing SWE magnitude, which is related to the inability of passive microwaves to penetrate deep snowpacks. This issue inhibits the ability of passive microwave retrievals to accurately estimate deep snowpack. The sampling frequency of AMSR-E is not sufficient to observe all global snowfall features simultaneously and accumulated monthly averages are used to capture the general pattern of snowfall, which is still underestimated. AMSR-E lacks channels above 90 GHz that are more sensitive to snowfall properties, which does have an impact on the retrieval. Results show that snow closure is achieved in the AMSR-E snow products, but the regions of closure are not necessarily regions of accurate snowfall and SWE observations to begin with.

The original intent of this study was to use closure arguments to assess where the products were already useful and where more work is needed. Perhaps the clearest conclusion from this study is that neither snowfall nor SWE is sufficiently consistent with each other or with other products to be globally useful at this time to improve global SWE estimates. Furthermore, the snowfall and SWE communities have operated independently, which does not allow for synergistic improvements. A coupled snowfall and SWE algorithm for spaceborne passive microwave retrievals will be able

to improve the current inconsistencies identified in this study. However, an important first step is improving the large underestimation of the initial representation of snowfall that would then be used to inform the subsequent SWE. In mountainous regions, the current snowfall algorithm suffers from the lack of information about small-scale precipitation processes, especially in regards to ice processes. An effective way to bridge the small-scale processes with course remotely sensed data could be to incorporate high-resolution model data into the *apriori* cloud profiles used in GPROF. Elsewhere, improvements to the current GPROF *apriori* database and high-latitude precipitation would be beneficial. Coupling the snowfall and SWE algorithms and improving the initial snowfall would allow for the improvement of both variables without having to separately develop each algorithm.

REFERENCES

Anderson, E. A., 1976: *A point energy and mass balance model of a snow cover*. U.S. Dept. of Commerce, National Oceanic and Atmospheric Administration, National Weather Service, Office of Hydrology, Silver Spring, Md., xviii, 150 p. pp., URL //catalog.hathitrust.org/Record/101642680.

Balk, B., and K. Elder, 2000: Combining binary decision tree and geostatistical methods to estimate snow distribution in a mountain watershed. *Water Resour. Res.*, **36 (1)**, 13–26, doi: 10.1029/1999WR900251, URL http://doi.wiley.com/10.1029/1999WR900251.

Barnett, T. P., J. C. Adam, and D. P. Lettenmaier, 2005: Potential impacts of a warming climate on water availability in snow-dominated regions. *Nature*, **438 (7066)**, 303–309, doi: 10.1038/nature04141, URL http://www.nature.com/articles/nature04141.

Betts, A. K., R. Desjardins, D. Worth, S. Wang, and J. Li, 2014: Coupling of winter climate transitions to snow and clouds over the Prairies. URL https://agupubs.onlinelibrary.wiley.com/doi/abs/10.1002/2013JD021168, doi: 10.1002/2013JD021168.

Bosilovich, M. G., J. Chen, F. R. Robertson, and R. F. Adler, 2008: Evaluation of Global Precipitation in Reanalyses. *J. Appl. Meteor. Climatol.*, **47 (9)**, 2279–2299, doi: 10.1175/2008JAMC1921.1, URL http://journals.ametsoc.org/doi/abs/10.1175/2008JAMC1921.1.

Brasnett, B., 1999: A Global Analysis of Snow Depth for Numerical Weather Prediction. *JOURNAL OF APPLIED METEOROLOGY*, **38**, 15.

Broxton, P. D., X. Zeng, and N. Dawson, 2016: Why Do Global Reanalyses and Land Data Assimilation Products Underestimate Snow Water Equivalent? *J. Hydrometeor.*, **17 (11)**, 2743–2761, doi: 10.1175/JHM-D-16-0056.1, URL http://journals.ametsoc.org/doi/10.1175/JHM-D-16-0056.1.

Carroll, T., D. Cline, G. Fall, A. Nilsson, L. Li, and A. Rost, 2001: NOHRSC OPERATIONS AND THE SIMULATION OF SNOW COVER PROPERTIES FOR THE COTERMINOUS U.S. 14.

Chang, A. T. C., J. L. Foster, and D. K. Hall, 1987: NIMUBUS-7 SMMR DERIVED GLOBAL SNOW COVER PARAMETERS. **9**, 39–44.

Cohen, J., and D. Rind, 1991: The Effect of Snow Cover on the Climate. *Journal of Climate*, **4 (7)**, 689–706, URL https://www.jstor.org/stable/26196419.

Dawson, N., P. Broxton, X. Zeng, M. Leuthold, M. Barlage, and P. Holbrook, 2016: An Evaluation of Snow Initializations in NCEP Global and Regional Forecasting Models. *J. Hydrometeor*, **17 (6)**, 1885–1901, doi: 10.1175/JHM-D-15-0227.1, URL http://journals.ametsoc.org/doi/10.1175/JHM-D-15-0227.1.

Derksen, C., and M. MacKay, 2006: The Canadian boreal snow water equivalent band. *Atmosphere-Ocean*, **44 (3)**, 305–320, doi: 10.3137/ao.440307, URL http://www.tandfonline.com/doi/abs/10.3137/ao.440307.

Ding, J., L. Bi, P. Yang, G. W. Kattawar, F. Weng, Q. Liu, and T. Greenwald, 2017: Single-scattering properties of ice particles in the microwave regime: Temperature effect on the ice refractive index with implications in remote sensing. *Journal of Quantitative Spectroscopy and Radiative Transfer*, **190**, 26–37, doi: 10.1016/j.jqsrt.2016.11.026, URL https://linkinghub.elsevier.com/retrieve/pii/S0022407316306367.

Ebtehaj, A. M., and C. D. Kummerow, 2017: Microwave retrievals of terrestrial precipitation over snow-covered surfaces: A lesson from the GPM satellite: PRECIPITATION MICROWAVES OVER SNOW COVER. *Geophys. Res. Lett.*, **44 (12)**, 6154–6162, doi: 10.1002/2017GL073451, URL http://doi.wiley.com/10.1002/2017GL073451.

Erxleben, J., K. Elder, and R. Davis, 2002: Comparison of spatial interpolation methods for estimating snow distribution in the Colorado Rocky Mountains. *Hydrol. Process.*, **16 (18)**, 3627–3649, doi: 10.1002/hyp.1239, URL http://doi.wiley.com/10.1002/hyp.1239.

Fassnacht, S. R., K. A. Dressler, and R. C. Bales, 2003: Snow water equivalent interpolation for the Colorado River Basin from snow telemetry (SNOTEL) data: SNOW WATER EQUIVALENT FROM SNOTEL DATA. *Water Resour. Res.*, **39 (8)**, doi: 10.1029/2002WR001512, URL http://doi.wiley.com/10.1029/2002WR001512.

Foster, J. L., A. T. C. Chang, and D. K. Hall, 1997: Comparison of Snow Mass Estimates from a Prototype Passive Microwave Snow Algorithm, a Revised Algorithm and a Snow Depth Climatology. *Remote Sensing of Environment*, **62**, 132–142.

Hancock, S., B. Huntley, R. Ellis, and R. Baxter, 2014: Biases in Reanalysis Snowfall Found by Comparing the JULES Land Surface Model to GlobSnow. *J. Climate*, **27 (2)**, 624–632, doi: 10.1175/JCLI-D-13-00382.1, URL http://journals.ametsoc.org/doi/abs/10.1175/JCLI-D-13-00382.1.

Jordan, R., 1990: A One-Dimensional Temperature Model for a Snow Cover. 62.

Kaatz, L., D. Yates, and M. Woodbury, 2008: The Joint Front Range Climate Change Vulnerability Study: Closing the Gap between Science and Water Management Decisions. *AGU Fall Meeting Abstracts*, GC33B-0777.

Kelly, R., 2009: The AMSR-E Snow Depth Algorithm: Description and Initial Results. **29 (1)**, 307–317.

Kongoli, C., H. Meng, J. Dong, and R. Ferraro, 2018: A hybrid snowfall detection method from satellite passive microwave measurements and global forecast weather models. *Q J R Meteorol Soc*, **144 (S1)**, 120–132, doi: 10.1002/qj.3270, URL https://onlinelibrary.wiley.com/doi/abs/10.1002/qj.3270.

Kongoli, C., P. Pellegrino, R. R. Ferraro, N. C. Grody, and H. Meng, 2003: A new snowfall detection algorithm over land using measurements from the Advanced Microwave Sounding Unit (AMSU): SNOWFALL DETECTION FROM AMSU. *Geophys. Res. Lett.*, **30 (14)**, doi: 10.1029/2003GL017177, URL http://doi.wiley.com/10.1029/2003GL017177.

Kummerow, C., 1994: A Passive Microwave Technique for Estimating Rainfall and Vertical Structure Information from Space, Part 1: Algorithm Description. **33**, 2–18, URL https://journals.ametsoc.org/doi/pdf/10.1175/1520-0450%281994%29033%3C0003%3AAPMTFE%3E2.0.CO%3B2.

Kummerow, C., W. Olson, and L. Giglio, 1996: A simplified scheme for obtaining precipitation and vertical hydrometeor profiles from passive microwave sensors. *IEEE Trans. Geosci. Remote Sensing*, **34 (5)**, 1213–1232, doi: 10.1109/36.536538, URL http://ieeexplore.ieee.org/document/536538/.

Kummerow, C. D., D. L. Randel, M. Kulie, N.-Y. Wang, R. Ferraro, S. Joseph Munchak, and V. Petkovic, 2015: The Evolution of the Goddard Profiling Algorithm to a Fully Parametric Scheme. *J. Atmos. Oceanic Technol.*, **32 (12)**, 2265–2280, doi: 10.1175/JTECH-D-15-0039.1, URL http://journals.ametsoc.org/doi/10.1175/JTECH-D-15-0039.1.

Kuo, K.-S., and Coauthors, 2016: The Microwave Radiative Properties of Falling Snow Derived from Nonspherical Ice Particle Models. Part I: An Extensive Database of Simulated Pristine Crystals and Aggregate Particles, and Their Scattering Properties. *Journal of Applied Meteorology and Climatology*, **55 (3)**, 691–708, doi: 10.1175/JAMC-D-15-0130.1, URL http://journals.ametsoc.org/doi/10.1175/JAMC-D-15-0130.1.

Libbrecht, K. G., 2007: The Formation of Snow Crystals. 9.

Liston, G. E., 1995: Local Advection of Momentum, Heat, and Moisture during the Melt of Patchy Snow Covers. *J. Appl. Meteor.*, **34**, 1705–1715.

Liston, G. E., and K. Elder, 2006a: A Distributed Snow-Evolution Modeling System (SnowModel). *J. Hydrometeor*, **7 (6)**, 1259–1276, doi: 10.1175/JHM548.1, URL http://journals.ametsoc.org/doi/abs/10.1175/JHM548.1.

Liston, G. E., and K. Elder, 2006b: A Meteorological Distribution System for High-Resolution Terrestrial Modeling (MicroMet). *Journal of Hydrometeorology*, **7 (2)**, 217–234, doi: 10.1175/JHM486.1, URL http://journals.ametsoc.org/doi/abs/10.1175/JHM486.1.

Liston, G. E., and D. K. Hall, 1995: An energy-balance model of lake-ice evolution. *J. Glaciol.*, **41**, 373–382.

Liston, G. E., and C. A. Hiemstra, 2008: A Simple Data Assimilation System for Complex Snow Distributions (SnowAssim). *Journal of Hydrometeorology*, **9 (5)**, 989–1004, doi: 10.1175/2008JHM871.1, URL http://journals.ametsoc.org/doi/abs/10.1175/2008JHM871.1.

Liston, G. E., and C. A. Hiemstra, 2011: The Changing Cryosphere: Pan-Arctic Snow Trends (1979âĂŞ2009). *Journal of Climate*, **24 (21)**, 5691–5712, doi: 10.1175/JCLI-D-11-00081.1,

URL http://journals.ametsoc.org/doi/abs/10.1175/JCLI-D-11-00081.1.

Liston, G. E., and M. Sturm, 1998: A snow-transport model for complex terrain. *Journal of Glaciology*, **44 (148)**, 498âĂŞ516, doi: 10.3189/S0022143000002021.

Liu, G., 2008: A Database of Microwave Single-Scattering Properties for Nonspherical Ice Particles. *Bull. Amer. Meteor. Soc.*, **89 (10)**, 1563–1570, doi: 10.1175/2008BAMS2486.1, URL http://journals.ametsoc.org/doi/10.1175/2008BAMS2486.1.

López-Moreno, J. I., and D. Nogués-Bravo, 2006: Interpolating local snow depth data: an evaluation of methods. *Hydrol. Process.*, **20 (10)**, 2217–2232, doi: 10.1002/hyp.6199, URL http://doi.wiley.com/10.1002/hyp.6199.

Masiokas, M. H., R. Villalba, B. H. Luckman, C. Le Quesne, and J. C. Aravena, 2006: Snowpack Variations in the Central Andes of Argentina and Chile, 1951âĂŞ2005: Large-Scale Atmospheric Influences and Implications for Water Resources in the Region. *Journal of Climate*, **19 (24)**, 6334–6352, doi: 10.1175/JCLI3969.1, URL http://journals.ametsoc.org/doi/abs/10.1175/JCLI3969.1.

McNeeley, S. M., T. A. Beeton, and D. S. Ojima, 2016: Drought Risk and Adaptation in the Interior United States: Understanding the Importance of Local Context for Resource Management in Times of Drought*. *Weather, Climate, and Society*, **8 (2)**, 147–161, doi: 10.1175/WCAS-D-15-0042.1, URL http://journals.ametsoc.org/doi/10.1175/WCAS-D-15-0042.1.

Meng, H., J. Dong, R. Ferraro, B. Yan, L. Zhao, C. Kongoli, N.-Y. Wang, and B. Zavodsky, 2017: A 1dvar-based snowfall rate retrieval algorithm for passive microwave radiometers: Microwave Snowfall Rate Algorithm. *J. Geophys. Res. Atmos.*, **122 (12)**, 6520–6540, doi: 10.1002/2016JD026325, URL http://doi.wiley.com/10.1002/2016JD026325.

Meyer, L., S. Brinkman, L. van Kesteren, N. Leprince-Ringuet, and F. van Boxmeer, 2014: Technical Support Unit for the Synthesis Report. 169.

Milly, P. C. D., K. A. Dunne, and A. V. Vecchia, 2005: Global pattern of trends in streamflow and water availability in a changing climate. *Nature*, **438 (7066)**, 347–350, doi: 10.1038/nature04312, URL http://www.nature.com/articles/nature04312.

Molotch, N. P., M. T. Colee, R. C. Bales, and J. Dozier, 2005: Estimating the spatial distribution of snow water equivalent in an alpine basin using binary regression tree models: the impact of digital elevation data and independent variable selection. *Hydrol. Process.*, **19 (7)**, 1459–1479, doi: 10.1002/hyp.5586, URL http://doi.wiley.com/10.1002/hyp.5586.

Mote, P. W., A. F. Hamlet, M. P. Clark, and D. P. Lettenmaier, 2005: DECLINING MOUNTAIN SNOWPACK IN WESTERN NORTH AMERICA*. *Bulletin of the American Meteorological Society*, **86 (1)**, 39–50, doi: 10.1175/BAMS-86-1-39, URL http://journals.ametsoc.org/doi/10.1175/BAMS-86-1-39.

Mudryk, L. R., C. Derksen, P. J. Kushner, and R. Brown, 2015: Characterization of Northern Hemisphere Snow Water Equivalent Datasets, 1981âĂŞ2010. *J. Climate*, **28 (20)**, 8037–8051, doi:

10.1175/JCLI-D-15-0229.1, URL http://journals.ametsoc.org/doi/10.1175/JCLI-D-15-0229.1.

Nakaya, U., 1951: The Formation of Ice Crystals. *Compendium of Meteorology: Prepared under the Direction of the Committee on the Compendium of Meteorology*, T. F. Malone, Ed., American Meteorological Society, Boston, MA, 207–220, doi: 10.1007/978-1-940033-70-9_18, URL https://doi.org/10.1007/978-1-940033-70-9_18.

NSIDC, 2012: All about snow. Accessed 4 September 2019. URL https://nsidc.org/cryosphere/snow.

Raleigh, M. S., J. D. Lundquist, and M. P. Clark, 2015: Exploring the impact of forcing error characteristics on physically based snow simulations within a global sensitivity analysis framework. *Hydrology and Earth System Sciences*, **19 (7)**, 3153–3179, doi: 10.5194/hess-19-3153-2015, URL https://www.hydrol-earth-syst-sci.net/19/3153/2015/.

Ray, A. J., 2008: A Synthesis to Support Water Resources Management and Adaptation. 58.

Reichle, R. H., C. S. Draper, Q. Liu, M. Girotto, S. P. P. Mahanama, R. D. Koster, and G. J. M. De Lannoy, 2017: Assessment of MERRA-2 Land Surface Hydrology Estimates. *J. Climate*, **30 (8)**, 2937–2960, doi: 10.1175/JCLI-D-16-0720.1, URL http://journals.ametsoc.org/doi/10.1175/JCLI-D-16-0720.1.

Reichle, R. H., R. D. Koster, G. J. M. De Lannoy, B. A. Forman, Q. Liu, S. P. P. Mahanama, and A. TourÃl', 2011: Assessment and Enhancement of MERRA Land Surface Hydrology Estimates. *J. Climate*, **24 (24)**, 6322–6338, doi: 10.1175/JCLI-D-10-05033.1, URL http://journals.ametsoc.org/doi/abs/10.1175/JCLI-D-10-05033.1.

Sims, E. M., and G. Liu, 2015: A Parameterization of the Probability of SnowâĂŞRain Transition. *J. Hydrometeor*, **16 (4)**, 1466–1477, doi: 10.1175/JHM-D-14-0211.1, URL http://journals.ametsoc.org/doi/10.1175/JHM-D-14-0211.1.

Stewart, I. T., D. R. Cayan, and M. D. Dettinger, 2005: Changes toward Earlier Streamflow Timing across Western North America. *Journal of Climate*, **18 (8)**, 1136–1155, doi: 10.1175/JCLI3321.1, URL http://journals.ametsoc.org/doi/abs/10.1175/JCLI3321.1.

Sturm, M., J. Holmgren, and G. E. Liston, 1995: A Seasonal Snow Cover Classification System for Local to Global Applications. **8**, 1261–1283, doi: 10.1175/JHM-D-15-0021.1.

Surussavadee, C., and D. H. Staelin, 2010: Global Precipitation Retrievals Using the NOAA AMSU Millimeter-Wave Channels: Comparisons with Rain Gauges. *J. Appl. Meteor. Climatol.*, **49 (1)**, 124–135, doi: 10.1175/2009JAMC2262.1, URL http://journals.ametsoc.org/doi/abs/10.1175/2009JAMC2262.1.

Takbiri, Z., A. Ebtehaj, E. Foufoula-Georgiou, P.-E. Kirstetter, and F. J. Turk, 2019: A Prognostic Nested *k* -Nearest Approach for Microwave Precipitation Phase Detection over Snow Cover. *J. Hydrometeor.*, **20 (2)**, 251–274, doi: 10.1175/JHM-D-18-0021.1, URL http://journals.ametsoc.org/doi/10.1175/JHM-D-18-0021.1.

Tedesco, M., and J. Jeyaratnam, 2016: A New Operational Snow Retrieval Algorithm Applied to Historical AMSR-E Brightness Temperatures. *Remote Sensing*, **8 (12)**, 1037, doi: 10.3390/rs8121037, URL http://www.mdpi.com/2072-4292/8/12/1037.

Tedesco, M., and P. S. Narvekar, 2010: Assessment of the NASA AMSR-E SWE Product. *IEEE Journal of Selected Topics in Applied Earth Observations and Remote Sensing*, **3 (1)**, 141–159, doi: 10.1109/JSTARS.2010.2040462.

Toure, A. M., M. Rodell, Z.-L. Yang, H. Beaudoing, E. Kim, Y. Zhang, and Y. Kwon, 2016: Evaluation of the Snow Simulations from the Community Land Model, Version 4 (CLM4). *Journal of Hydrometeorology*, **17 (1)**, 153–170, doi: 10.1175/JHM-D-14-0165.1, URL http://journals.ametsoc.org/doi/10.1175/JHM-D-14-0165.1.

Ulaby, F. T., and W. H. Stiles, 1980: The active and passive microwave response to snow parameters: 2. Water equivalent of dry snow. *J. Geophys. Res.*, **85 (C2)**, 1045, doi: 10.1029/JC085iC02p01045, URL http://doi.wiley.com/10.1029/JC085iC02p01045.

Vavrus, S., 2007: The role of terrestrial snow cover in the climate system. *Climate Dynamics*, **29 (1)**, 73–88, doi: 10.1007/s00382-007-0226-0, URL http://link.springer.com/10.1007/s00382-007-0226-0.

Walland, D. J., and I. Simmonds, 1996: *Modelled atmospheric response to changes in Northern Hemisphere snow cover*.

Xiao, Z., and A. Duan, 2016: Impacts of Tibetan Plateau Snow Cover on the Interannual Variability of the East Asian Summer Monsoon. *Journal of Climate*, **29 (23)**, 8495–8514, doi: 10.1175/JCLI-D-16-0029.1, URL http://journals.ametsoc.org/doi/10.1175/JCLI-D-16-0029.1.

You, Y., N.-Y. Wang, R. Ferraro, and S. Rudlosky, 2017: Quantifying the Snowfall Detection Performance of the GPM Microwave Imager Channels over Land. *J. Hydrometeor.*, **18 (3)**, 729–751, doi: 10.1175/JHM-D-16-0190.1, URL http://journals.ametsoc.org/doi/10.1175/JHM-D-16-0190.1.

Zeng, X., P. Broxton, and N. Dawson, 2018: Snowpack Change From 1982 to 2016 Over Conterminous United States. *Geophysical Research Letters*, **45**, 12 940–12 947, doi: 10.1029/2018GL079621, URL https://agupubs.onlinelibrary.wiley.com/doi/abs/10.1029/2018GL079621.

APPENDIX

Temporal Consistency in AMSR-E Snow Products

Throughout the paper, comparisons between products and datasets were given for February only. February is chosen to eliminate complications of AMSR-E retrieving SWE during snowmelt and to ease comparison in the products. This section provides comparisons for other months throughout the simulation year.

Figure A1 shows the average bias in each region as a function of time. As previously discussed, AMSR-E underestimates accumulated snowfall from July through February. The underestimation of snowfall is observed during the entirety of the winter season and the underestimation increases monotonically throughout the season. The biases propagate from month-to-month as the season progresses, but there is no large sensitivity to an increased biases at a certain time of the season.

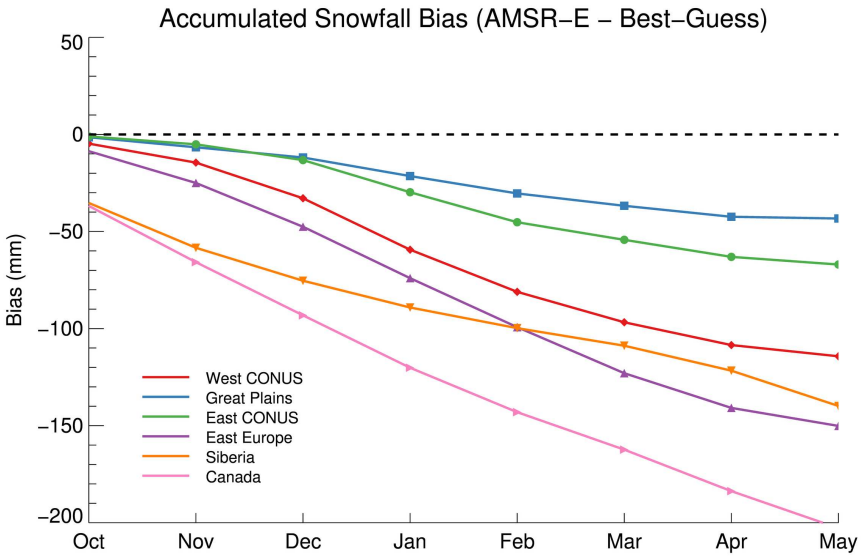

Fig. A1. Average monthly biases for the region of interest. Monthly snowfall data is averaged for all simulation years (2003-2011).

Figure A2 shows the average bias in each region as a function of time, and show a different temporal sensitivity than the temporal snowfall biases. Consistent temporal biases between AMSR-E SWE and the best-guess SWE product are observed in the Great Plains. The Western CONUS, Eastern CONUS, Eastern Europe all possess increasing underestimation as the season progresses. The Siberian region, a known problem area in the current AMSR-E SWE algorithm, overestimates SWE compared to the best-guess SWE product from December to March, which is related to fast metamorphism of snow grains early in the season in this region.

Similarly to the snowfall biases, there is a consistent underestimation of the average closure bias between the observed AMSR-E snowfall and inferred AMSR-E snowfall (Figure A3). In all regions besides Siberia, the closure bias is less than the snowfall bias seen in Figure A1. The closure biases appear to be lower in these regions because the AMSR-E SWE is underestimated, which effects the amount of inferred snowfall. This, however, is not the case for the Siberia region where the AMSR-E SWE is known to be severely overestimated.

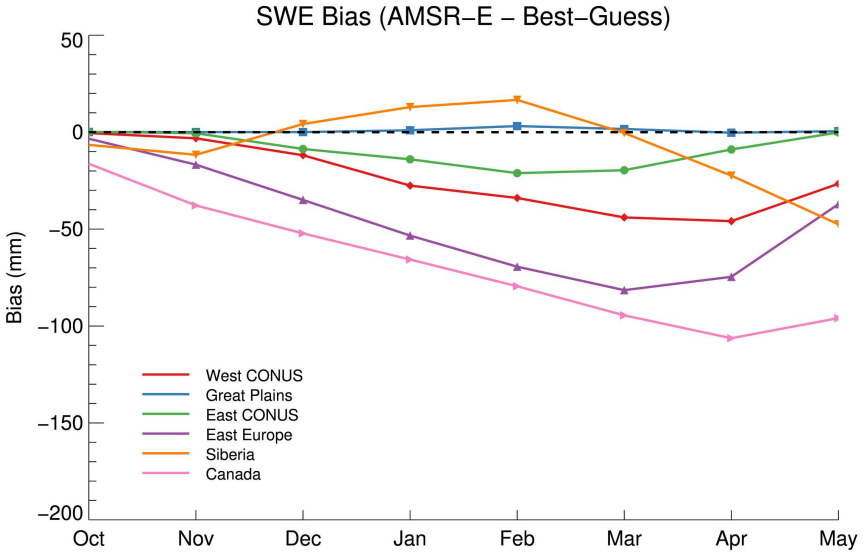

Fig. A2. Same as in Figure A1, but for SWE data.

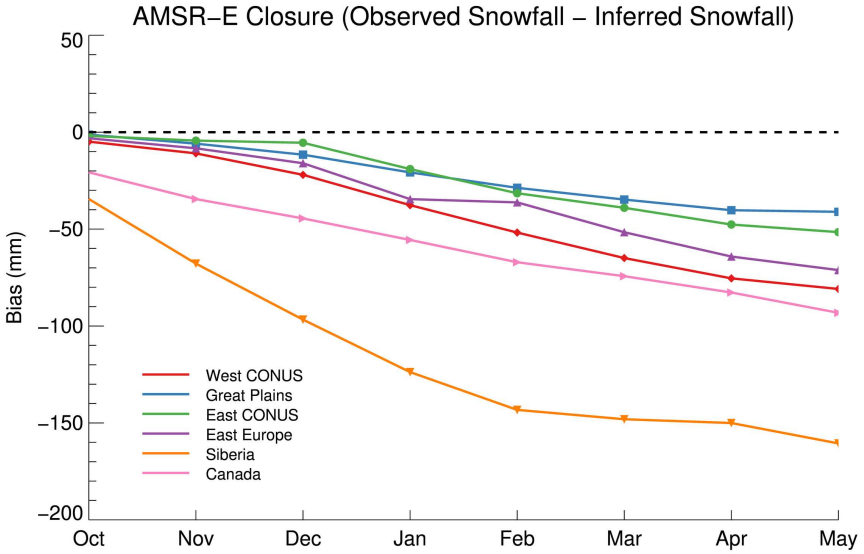

Fig. A3. Same as in Figure A1, but for closure data between AMSR-E observed snowfall and AMSR-E inferred snowfall.

During each simulation year, SnowAssim is used to correct the snowfall inputs so the modeled SWE matches the observed assimilated SWE. Correction factors are applied to the MERRA-2 snowfall. Mean global scaling factors for the assimilated months (October, December, February, and April) for all datasets are shown in Figure A4. Correction factors are not an indication of the overall bias between the SWE data, but rather the similarity between the required snowfall for each product. Correction factors are typically near unity while large deviations indicate significant

differences in the amount of snowfall that is required. The temporal variability in the mean global correction factors indicates there is no systematic bias in the datasets for all regions throughout the year. In general, AMSR-E and CMC have repeatable temporal patterns in their corresponding SWE data with an increase in mean correction factors as the winter season progresses. A large decrease in correction factor for April can be explained by AMSR-E's inability to measure SWE in wet, melting snowpacks. The patterns of AMSR-E and CMC correction factors suggest MERRA-2 overestimates the required global snowfall early in the season and underestimates global snowfall as the season progresses to mid-winter. MERRA-2 exhibits over and underestimation of CONUS precipitation throughout the winter season compared to SNODAS and is not consistent from year-to-year. The monthly mean correction factor standard deviations are highest for AMSR-E and lowest for SNODAS indicating a high amount of variance globally in the AMSR-E product.

The patterns in mean correction factors point to a systematic problem within the AMSR-E SWE product. The increase of mean correction factors for AMSR-E are related to the significant overestimation of SWE in regions influenced by large snow grains, especially in the Siberia region (Figure 3.9). The CMC and SNODAS products are more influenced by differences in the snow evolution model, observations, and meteorological forcing used in each product.

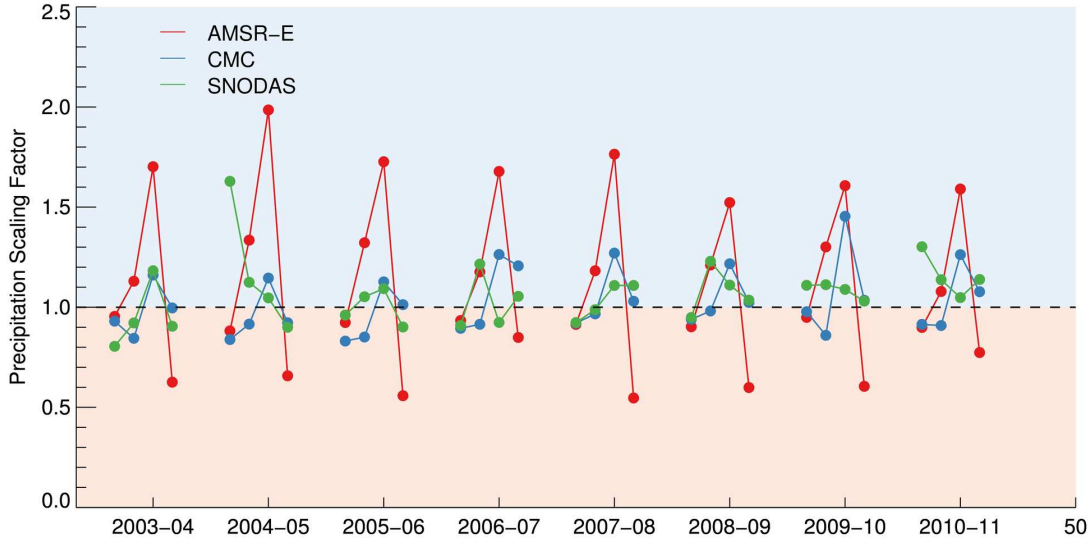

Fig. A4. Monthly, globally averaged SnowModel correction factors. Correction factors are computed by the SnowAssim submodel.